Autoinhibition and regulation by phosphoinositides of ATP8B1, a human lipid flippase associated with intrahepatic cholestatic disorders

Thibaud Dieudonné[a,1], Sara Abad Herrera[b#], Michelle Juknaviciute Laursen[c#], Maylis Lejeune[a,2], Charlott Stock[c], Kahina Slimani[a], Christine Jaxel[a], Joseph A. Lyons[d], Cédric Montigny[a], Thomas Günther Pomorski[b,e*], Poul Nissen[c*] and Guillaume Lenoir[a*]

[a] Université Paris-Saclay, CEA, CNRS, Institute for Integrative Biology of the Cell (I2BC), 91198, Gif-sur-Yvette, France

[b] Faculty of Chemistry and Biochemistry, Department of Molecular Biochemistry, Ruhr University Bochum, 44870, Bochum, Germany

[c] DANDRITE, Nordic EMBL Partnership for Molecular Medicine, Department of Molecular Biology and Genetics, Aarhus University, Aarhus, Denmark

[d] Department of Molecular Biology and Genetics, Aarhus University, Aarhus, Denmark

[e] Department of Plant and Environmental Sciences, University of Copenhagen, Frederiksberg, Denmark

[1] Current address: DANDRITE, Nordic EMBL Partnership for Molecular Medicine, Department of Molecular Biology and Genetics, Aarhus University, Aarhus, Denmark

[2] Current address: Institut Pasteur, Université de Paris, CNRS UMR3528, Structural Bioinformatics Unit, F-75015 Paris, France

[#] These authors contributed equally to this work

* Corresponding author; E-mail: thomas.guenther-pomorski@ruhr-uni-bochum.de

* Corresponding author; E-mail: pn@mbg.au.dk

* Corresponding author; E-mail: guillaume.lenoir@i2bc.paris-saclay.fr

Running title: Regulatory mechanism of the human flippase ATP8B1

Abstract

P-type ATPases from the P4 subfamily (P4-ATPases) are primary active transporters that maintain lipid asymmetry in eukaryotic cell membranes by flipping lipids from the exoplasmic to the cytosolic leaflet. Mutations in several human P4-ATPase genes are associated with severe diseases. For instance, mutations in the ATP8B1 gene result in progressive familial intrahepatic cholestasis, a rare inherited disorder that usually progresses toward liver failure. ATP8B1 forms a binary complex with CDC50A and displays a broad specificity to glycerophospholipids, but regulatory mechanisms are unknown. Here, we report the cryo-EM structure of the human lipid flippase ATP8B1-CDC50A at 3.1 Å resolution. The lipid flippase complex is autoinhibited by the N- and C-termini of ATP8B1, which in concert form extensive interactions with the catalytic sites and flexible domain interfaces of ATP8B1. Consistently, ATP hydrolysis by the ATP8B1-CDC50A complex requires truncation of its C-terminus as well as the presence of phosphoinositides, with a marked preference for phosphatidylinositol-3,4,5-phosphate (PI(3,4,5)P_3), and removal of both N- and C-termini results in full activation. Restored inhibition of ATP8B1 truncation constructs with a synthetic peptide mimicking the C-terminus further suggests molecular communication between N- and C-termini in the autoinhibition process and demonstrates that the regulatory mechanism can be interfered with by exogenous compounds. A conserved (G/A)(Y/F)AFS motif in the C-termini of several P4-ATPase subfamilies suggests that this mechanism is employed widely across P4-ATPase lipid flippases, including both plasma membrane and endomembrane P4-ATPases.

Keywords: Lipid transporter/Autoinhibition/Phosphoinositides/P4-ATPases/Progressive familial intrahepatic cholestasis/Cryo-EM

Author contributions: G.L. conceived the project. T.D., C.M., P.N., T.G.P. and G.L. designed research. T.D., M.L., S.A.H., C.J., M.J.L., K.S, and C.M. performed experiments. J.A.L. contributed protocols and reagents. T.D., M.L., C.S., S.A.H., J.A.L., P.N., T.G.P., C.M., and G.L. analyzed data. The manuscript was drafted by G.L. and T.D. All authors commented on the manuscript.

Introduction

Transbilayer lipid asymmetry is a fundamental characteristic of eukaryotic cell and organelle membranes (Kobayashi and Menon, 2018; van Meer, 2011; van Meer et al., 2008; Verkleij et al., 1973). In most cell types choline-containing phosphatidylcholine (PC) and sphingomyelin (SM) are chiefly located in the exoplasmic leaflet while the aminophospholipids phosphatidylserine (PS) and phosphatidylethanolamine (PE), as well as phosphoinositides (PPIns), mostly occupy the cytoplasmic leaflet (Bretscher, 1972; Murate et al., 2015). Phospholipid asymmetry plays an important role in eukaryotic cell function. A well-studied example is the asymmetric distribution of PS in membranes of the late secretory/endocytic pathways, where it confers a high surface charge to these membranes, thereby facilitating the recruitment of polybasic motif-containing protein effectors such as the small G proteins K-Ras (Hancock et al., 1990; Yeung et al., 2009), Cdc42 and ROP6, as well as other proteins like protein kinase C (PKC), synaptotagmin, and the membrane fission protein EHD1 (Bohdanowicz and Grinstein, 2013; Lee et al., 2015; Lemmon, 2008; Leventis and Grinstein, 2010; Platre et al., 2019). Thus, there is a direct link between PS sidedness and regulation of cell polarity, cell signaling and vesicular trafficking. Phospholipid asymmetry is maintained by flippases and floppases, which use ATP for inward and outward movement of lipids across membranes, respectively (Andersen et al., 2016; López-Marqués et al., 2015; Montigny et al., 2016). In contrast, scramblases comprise a third category that passively equilibrates lipids across the bilayer, often controlled by gating (Pomorski and Menon, 2016). Whereas floppases belong to the superfamily of ATP-binding cassette (ABC) transporters, most flippases characterized thus far are from the type 4 subfamily of P-type ATPases, hereafter referred to as P4-ATPases. Similar to many ion-transporting P-type ATPases, P4-ATPases consist of a transmembrane domain containing ten membrane-spanning α-helical segments, as well as three cytosolic domains, the actuator (A), nucleotide-binding (N), and phosphorylation (P) domains involved in catalysis (Fig. 1A). Importantly, most P4-ATPases form obligatory binary complexes with members of the CDC50 protein family, which are essential for correct targeting of the flippase complex to its final destination and for its transport activity (Coleman and Molday, 2011; Lenoir et al., 2009; Poulsen et al., 2008; Saito et al., 2004; Segawa et al., 2018). Conformational changes in the membrane domain, required to facilitate lipid transport, are coupled to phosphorylation and dephosphorylation events in the cytosolic ATPase domains, thereby allowing efficient lipid transport against concentration gradients. The different steps of the transport cycle are collectively described as the Post-Albers scheme (Albers, 1967; Post et al., 1972), where the P-type ATPase cycles between different conformations, E1, E1P, E2P and E2 (P for phosphorylated) (Fig. 1B). The transport substrate, a lipid for P4-ATPases, is recognized

105 in the E2P conformation, and its binding triggers dephosphorylation leading to E2 and eventually
106 release of the lipid in the opposing leaflet. Recent high-resolution structures of the yeast Drs2-Cdc50,
107 Dnf1,2-Lem3 and the human ATP8A1-CDC50A and ATP11C-CDC50A flippase complexes have
108 illuminated the molecular mechanism of lipid transport, providing a framework for understanding how
109 these transporters are able to move lipids (Bai et al., 2020, 2019; Hiraizumi et al., 2019; Lyons et al.,
110 2020; Nakanishi et al., 2020; Timcenko et al., 2021, 2019). A key feature that has emerged from
111 these high-resolution structures is the mechanism by which the C-terminus of yeast Drs2 and human
112 ATP8A1 autoinhibits their respective activities (Hiraizumi et al., 2019; Timcenko et al., 2019).
113 Furthermore, structures obtained in the presence of phosphatidylinositol-4-phosphate (PI(4)P) shed
114 light on the specific regulation of Drs2 by this phosphoinositide, as previously observed using purified
115 enzyme and activity assays (Azouaoui et al., 2017; Natarajan et al., 2009; Zhou et al., 2013).
116 The human genome encodes 14 P4-ATPases. Mutations in ATP8A2 and ATP11A have been
117 reported to cause severe neurological disorders (Onat et al., 2013; Segawa et al., 2021) while
118 mutations in ATP8B1 are associated with intrahepatic cholestatic disorders, such as benign
119 recurrent intrahepatic cholestasis (BRIC1), intrahepatic cholestasis of pregnancy (ICP1), and the
120 more severe progressive familial intrahepatic cholestasis type 1 (PFIC1). PFIC1 is a rare inherited
121 liver disorder characterized by impaired bile flow, fat malabsorption and progressive cirrhosis and
122 fibrosis (Jacquemin, 2012; van der Mark et al., 2013). The subcellular localization, heteromeric
123 interactions with CDC50 proteins and lipid transport activity of ATP8B1 have been thoroughly
124 investigated using cell-based assays (Bryde et al., 2010; Takatsu et al., 2014; van der Velden et al.,
125 2010). In contrast, ATP8B1 remains poorly studied from a molecular standpoint. In particular, while
126 several other P4-ATPases, and P-type ATPases in general, are tightly regulated by lipid co-factors,
127 protein partners, or by their terminal extensions (Azouaoui et al., 2017; Chalat et al., 2017; Holemans
128 et al., 2015; Saffioti et al., 2021; Tsai et al., 2013), the way ATP8B1 activity is regulated remains
129 unknown.
130 In this report, we purified human ATP8B1-CDC50A complex, amenable for detailed study of its three-
131 dimensional structure and catalytic activity. We determined the high-resolution structure of an
132 autoinhibited ATP8B1-CDC50A by cryo-electron microscopy (cryo-EM). In keeping with the binding
133 mode of the C-terminal tail of ATP8B1 with the cytosolic domains, the ATP8B1-CDC50A complex
134 displayed ATPase activity only after removal of its C-terminus. Using protease cleavage sites within
135 the N-terminus or immediately after the last transmembrane segment of ATP8B1, we demonstrate
136 that ATP8B1 is primarily autoinhibited by its C-terminal extension, but that the N-terminal extension
137 is involved in a synergistic manner. In addition to the importance of these autoregulatory elements,
138 we show that PPIns are critical activators of ATP8B1 activity.

Results

Cryo-EM structure of the ATP8B1-CDC50A complex in the autoinhibited E2P state

Recent studies revealed that flippases can be autoregulated by their terminal extensions. In particular, (G/A)(Y/F)AFS motifs in the C-termini of Drs2 and ATP8A1 occupy the nucleotide binding site, thereby preventing conformational changes required for lipid transport (Hiraizumi et al., 2019; Timcenko et al., 2019). This motif is well-conserved also in ATP8B1 as ^{1208}AYAF^{1212}S (Fig. 1A), suggesting a regulatory role of the ATP8B1 C-terminus. To gain insight into the mechanism of ATP8B1 regulation, we devised a procedure for co-overexpression of ATP8B1 and CDC50A in *Saccharomyces cerevisiae* and purification of the complex (Fig. S1A and S1B). ATP8B1 and CDC50A co-expressed well in yeast and were solubilized from yeast membranes using n-Dodecyl-β-D-Maltoside (DDM) supplemented with cholesteryl hemisuccinate (CHS). Following streptavidin-based affinity chromatography and on-column cleavage of the biotin acceptor domain (BAD) tag with TEV protease, we obtained a highly pure ATP8B1-CDC50A complex (Fig. 1C and Fig. S1C). Treatment of the purified ATP8B1-CDC50A complex with Endoglycosidase H resulted in consolidation of multiple bands into a single band around 40 kDa, the expected molecular weight of histidine-tagged CDC50A, reflecting various glycosylation levels of its polypeptide chain (Fig. S1C). The stoichiometry between ATP8B1 and CDC50A was found to be 1:1, as determined by in-gel fluorescence (Fig. S1D and S1E). P-type ATPases couple autophosphorylation from ATP and subsequent dephosphorylation of a catalytic aspartate in the P-domain to structural changes in the membrane domain, thus transporting substrates across the membrane against steep concentration gradients (Fig. 1B). To ascertain functionality of the purified complex, we investigated its ability to undergo phosphorylation from [γ-^{32}P]ATP on its catalytic aspartate. The results confirm that the phosphoenzyme involves formation of an aspartyl-phosphate bond on residue D454 (Fig. 1D). For structural studies, DDM was exchange for lauryl maltose neopentyl glycol (LMNG). The resulting sample showed a high degree of monodispersity on size-exclusion chromatography (Fig. 1E).

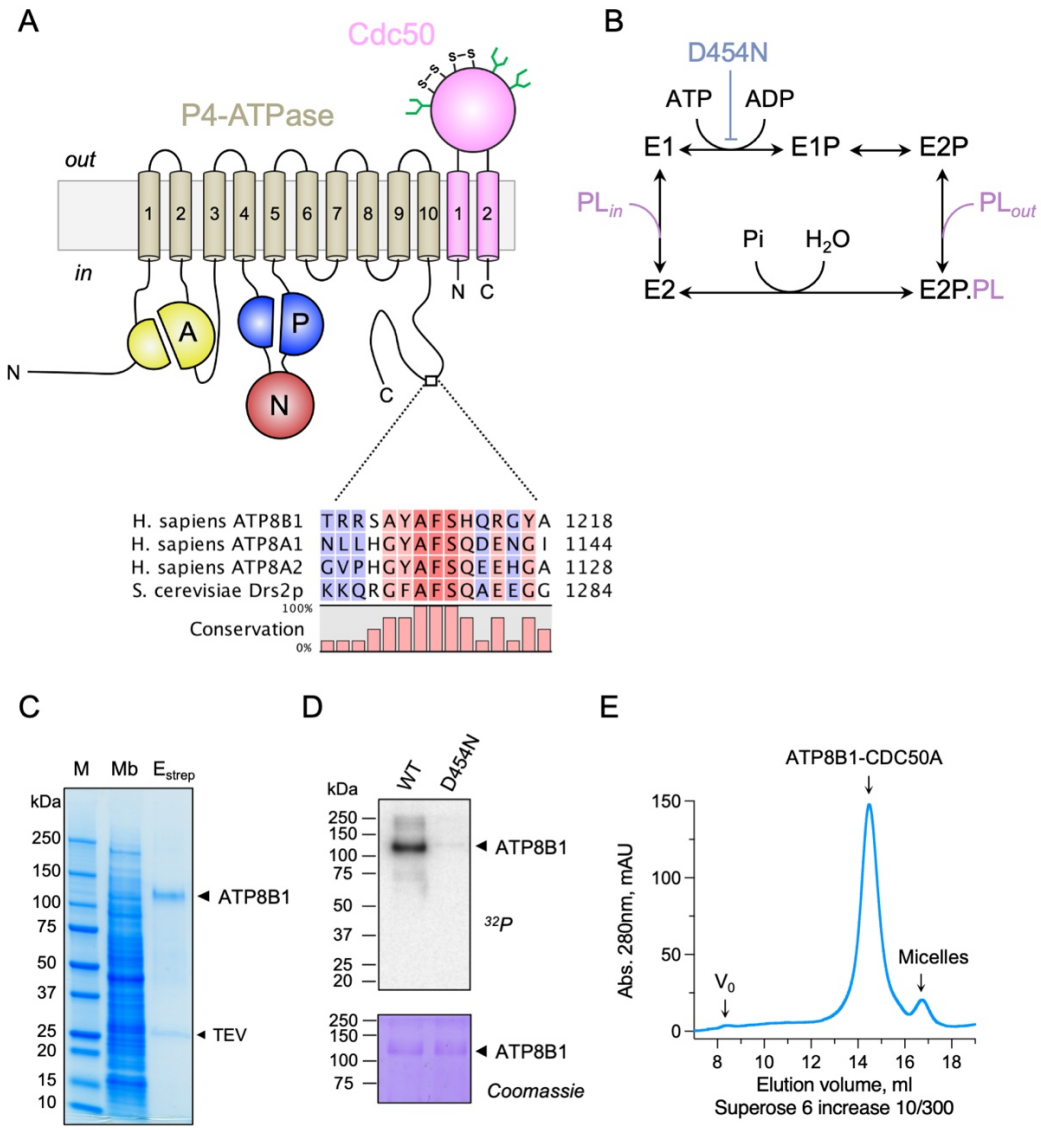

Figure 1 – Purification and functional assessment of the ATP8B1-CDC50A complex expressed in *Saccharomyces cerevisiae*.

(A) Predicted topology of ATP8B1-CDC50A with the transmembrane domain of ATP8B1 in tan and the Actuator domain (A), the Nucleotide binding domain (N) and the Phosphorylation domain (P) in yellow, red, and blue, respectively. CDC50A with two transmembrane spans and a large exoplasmic loop in pink; predicted disulfide bridges (S-S) and glycosylation sites (green) are indicated. Sequence alignment of part of the C-terminus of ATP8B1, ATP8A1, ATP8A2, and Drs2 (CLC, Qiagen). The shading indicates conservation (blue 0% – red 100%). Accession numbers are P39524 for Drs2, Q9Y2Q0 for ATP8A1, Q9NTI2 for ATP8A2 and O43520 for ATP8B1. *(B)* Post-Albers cycle for P4-ATPases. ATP8B1 mutation D454N prevents phosphorylation on the catalytic aspartate and thus blocks activity. Pi, inorganic phosphate; PL, phospholipid. *(C)* SDS-PAGE analysis of ATP8B1-CDC50A affinity purification on streptavidin beads. Proteins contained in crude yeast membranes (Mb) and recovered upon TEV protease cleavage on streptavidin beads (E_{strep}) were visualized by Coomassie Blue staining. M, molecular weight marker. *(D)* Phosphoenzyme formation from [γ-^{32}P]ATP of wild-type and catalytically-inactive D454N variant, as analyzed after electrophoretic separation on acidic gels. Coomassie Blue staining of the same gel was used to control the amount of wild-type and D454N subjected to ^{32}P labeling. *(E)* Size-exclusion chromatography elution profile of the purified human ATP8B1-CDC50A complex used for cryo-EM studies. Arrows indicate the void volume of the column (v_0), as well as the elution volume of the ATP8B1-CDC50A complex and detergent micelles.

185

186 The structure of the full-length complex was then determined using single particle cryo-EM. To
187 stabilize the complex in the autoinhibited E2P conformation ($E2P_{autoinhibited}$), the sample was
188 incubated in the presence of beryllium fluoride (BeF_3^-, $BeF_2(OH)_2$ referred to as BeF_x) mimicking
189 phosphorylation. The high-resolution map (overall resolution: 3.1Å) obtained by cryo-EM enabled us
190 to model most of ATP8B1 and CDC50A sequences (Fig. 2 and Table S1), except flexible loops and
191 termini. As expected, ATP8B1 harbors a typical P4-ATPase fold with a transmembrane helical
192 bundle made of 10 α-helical segments, a nucleotide binding domain (N), a phosphorylation domain
193 (P) and an actuator domain (A). Comparison with other P4-ATPase structures and the presence of
194 an extra density in the phosphorylation site confirmed that our structure resembles an $E2P_{autoinhibited}$
195 state with bound BeF_x (Fig. S2). In addition, the cryo-EM data displayed very clear densities for parts
196 of the N- and C-termini of ATP8B1 (Fig. 3). Interestingly, the N-terminal region (Q16-D26) was found
197 to interact tightly with the P- and the A-domain of ATP8B1. The C-terminal tail of ATP8B1 was found
198 to interact with the P-, N-, and A-domains, while the last 23 residues were not resolved in the cryo-
199 EM map likely due to a high degree of flexibility (Fig. 3).
200

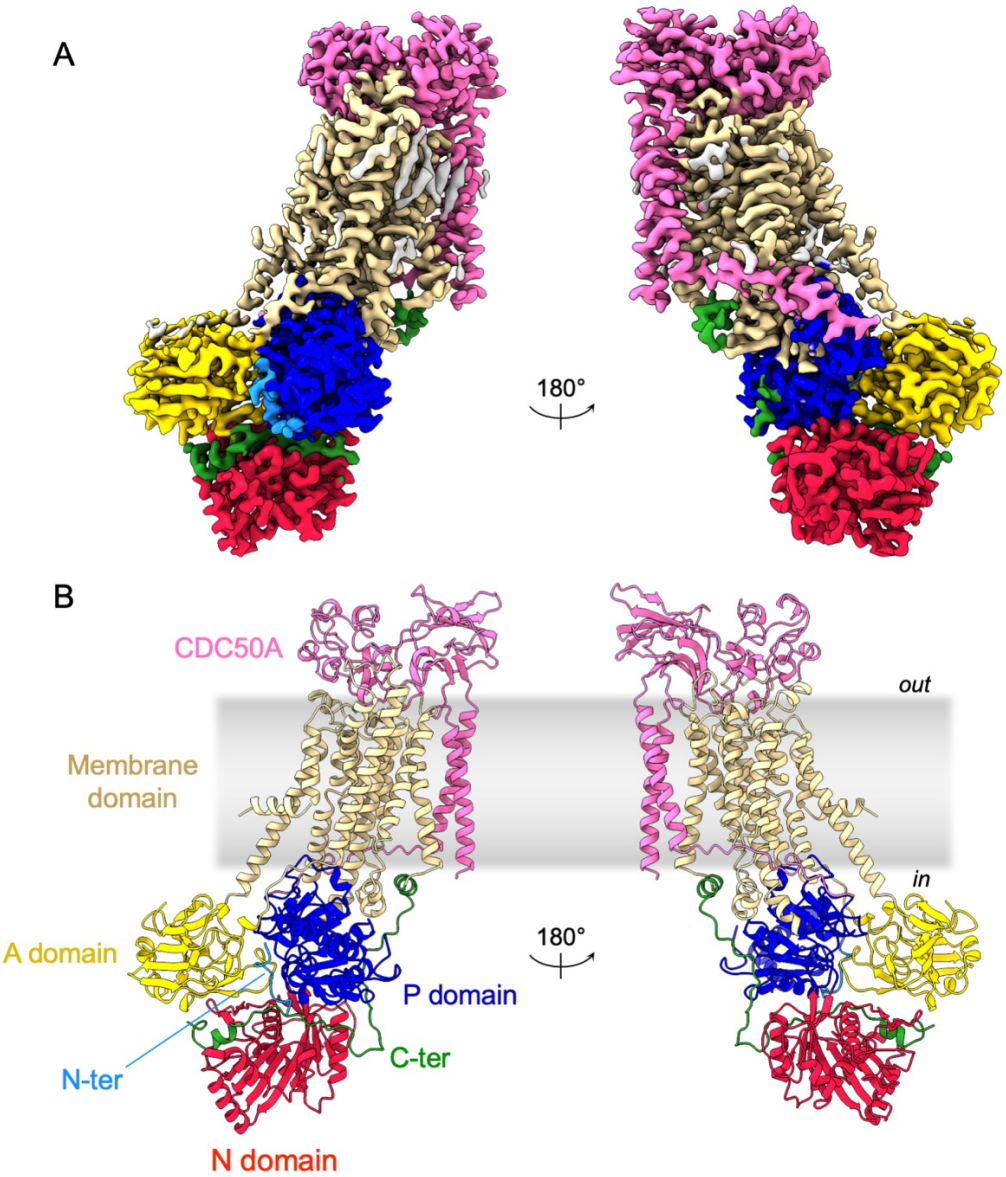

Figure 2 – Overall ATP8B1-CDC50A structure.
(A) Cryo-EM map of ATP8B1-CDC50A in the E2P autoinhibited state. The cytosolic A-, N- and P-domains of ATP8B1 are colored in yellow, red and blue, respectively. The transmembrane domain of ATP8B1 is colored in tan. The N- and C-terminal tails of ATP8B1 are colored in cyan and green, respectively. CDC50A is colored in pink. CHS densities and residual densities corresponding to detergent or less ordered unmodelled lipids are in grey. *(B)* Cartoon representation of the refined model. Colors are as in *(A)*.

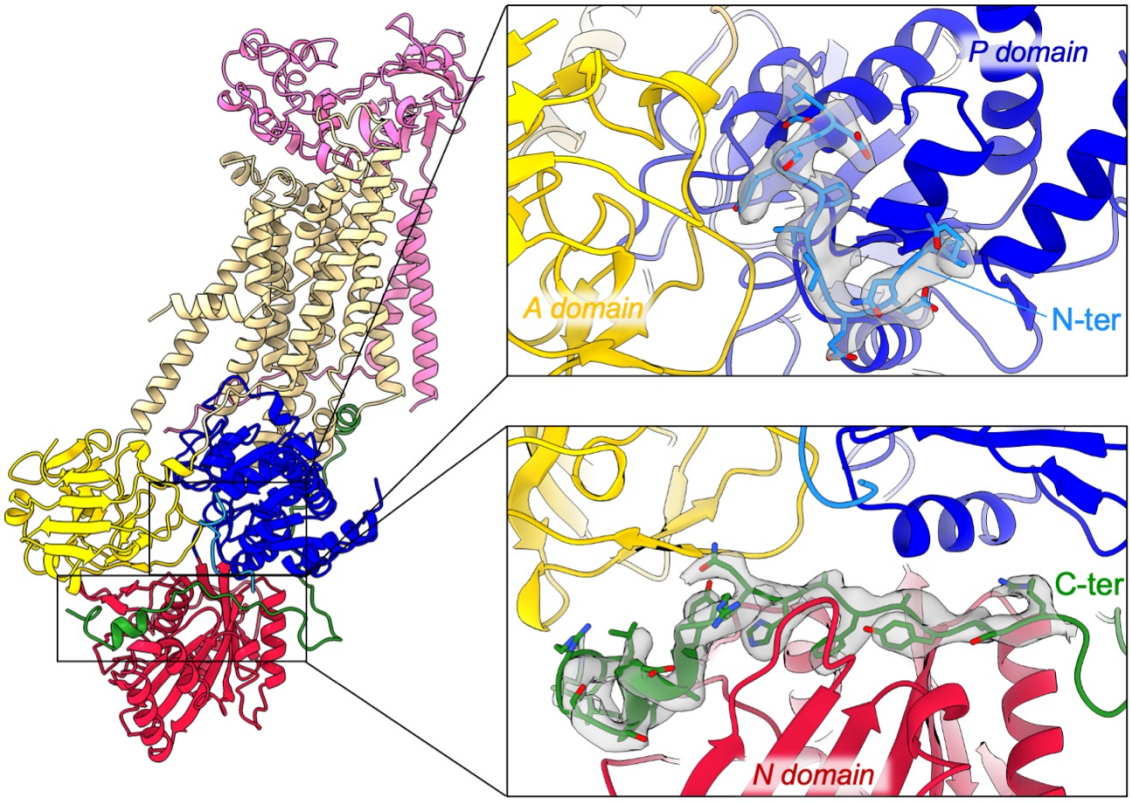

209

210 **Figure 3 – Detailed interaction of ATP8B1-CDC50A N- and C-terminal tails with the cytosolic A-, N- and**
211 **P-domains.**
212 Overall and close-up views of the N- and C-terminal tails and their corresponding electron densities. The
213 cytosolic A-, N- and P-domains of ATP8B1 are colored in yellow, red and blue, respectively. The
214 transmembrane domain of ATP8B1 is colored in tan. The N- and C-terminal tails of ATP8B1 and their side
215 chains are colored in cyan and green, respectively. CDC50A is colored in pink.
216

217

218 **Autoinhibition of ATP8B1 by its N- and C-termini**

219 To investigate the role of ATP8B1 N- and C-termini, we inserted 3C protease cleavage sites after
220 residue P42 in the N-terminus, to remove most of the N-terminal tail including the Q16-D26 region
221 found in the structure, and/or after residue E1174 at the end of the last transmembrane segment 10,
222 to remove the C-terminus (Fig. S3). The various 3C protease constructs were purified by streptavidin
223 affinity chromatography (Fig. 4A). Noteworthy, insertion of the 3C protease cleavage sites did not
224 alter the interaction between ATP8B1 and CDC50A, as shown by immunoblotting of the fraction
225 collected upon incubation of streptavidin beads with 3C and TEV (Fig. S4A). Removal of the N-
226 terminus and/or the C-terminus was not sufficient to stimulate ATP8B1-CDC50A ATPase activity in
227 the presence of its transport substrate PC, suggesting an additional regulatory mechanism (Fig. 4B).
228 PI(4)P has been shown to be essential to stimulate ATP hydrolysis by Drs2, a yeast homolog of
229 ATP8B1 (Azouaoui et al., 2017). Considering that ATP8B1 is localized at the plasma membrane
230 (PM), we reasoned that addition of PI(4,5)P_2, the most abundant phosphoinositide in the PM (Balla,

2013; Dickson and Hille, 2019), might be required to elicit ATP8B1 activity. As displayed in Fig. 4B, we observed a ~ four-fold increase in ATP hydrolysis upon addition of PI(4,5)P_2, for the C-terminally truncated construct. Interestingly, removal of both termini resulted in additional activation of ATP8B1 suggesting that, although the sole removal of the N-terminus is not sufficient to relieve autoinhibition, the N-terminus cooperates with the C-terminus for autoinhibition of the ATP8B1-CDC50A complex (Fig. 4B). Addition of BeF_x inhibited the ATPase activity of ATP8B1 with an IC_{50} of ~45 μM, consistent with the ability of this structural analog of phosphate to act as a general P-type ATPase inhibitor (Fig. S4B) (Danko et al., 2009). Finally, the purified ATP8B1-CDC50A complex showed a K_m of ~ 40 μM for MgATP (Fig. S4C).

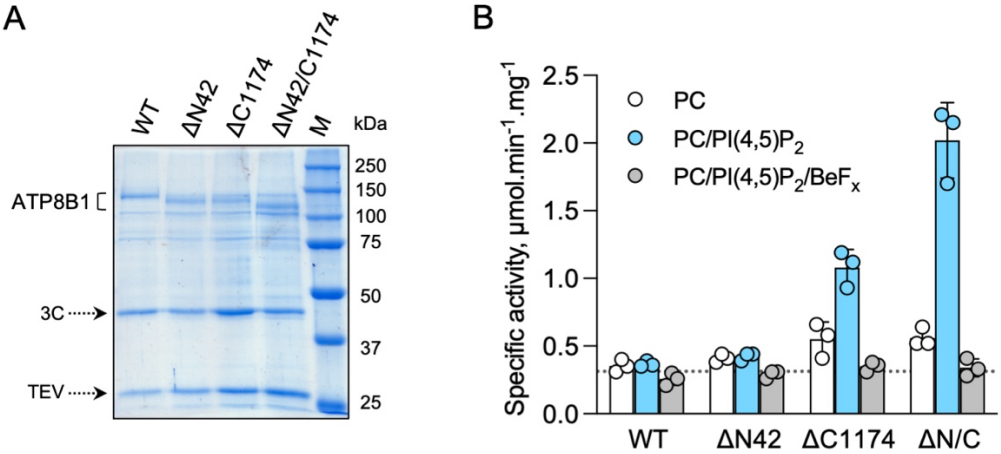

Figure 4 - ATP8B1-CDC50A is autoinhibited by both its N- and C-terminal tails, and the presence of lipids is required for its activity.
(A) Efficient removal of N- and/or C-terminal extensions of ATP8B1 upon on-column cleavage of ATP8B1-CDC50A with both TEV and 3C proteases assessed by Coomassie blue stained SDS-PAGE. ΔN42 lacks residues 1-42 of ATP8B1 whereas ΔC1174 lacks residues 1175-1251 and ΔN42/C1174 lacks both. M, molecular weight marker. *(B)* ATPase activity of wild-type (WT), N-terminally truncated (ΔN42), C-terminally truncated (ΔC1174) and both N- and C-terminally truncated (ΔN42/C1174) ATP8B1 (~ 5 μg ml^{-1} protein) in complex with CDC50A determined in DDM at 30°C. Data are a mean ± s.d. of 3 replicate experiments. The dotted line represents background NADH oxidation measured in the absence of purified protein and lipids.

To more precisely assess the involvement of the ATP8B1 C-terminal region in autoinhibition, we asked whether addition of a peptide mimicking the C-terminus of ATP8B1 inhibited the enzyme. To answer this question, a peptide encompassing the AYAFS motif (residues 1205-1251, Fig. S3) was chemically synthesized and incubated with ΔN42/ΔC1174 ATP8B1. Fig. 5A shows that this C-terminal peptide efficiently inhibited ATP hydrolysis by ATP8B1, with an IC_{50} of ~ 22 μM (Fig. 5A and 5B).

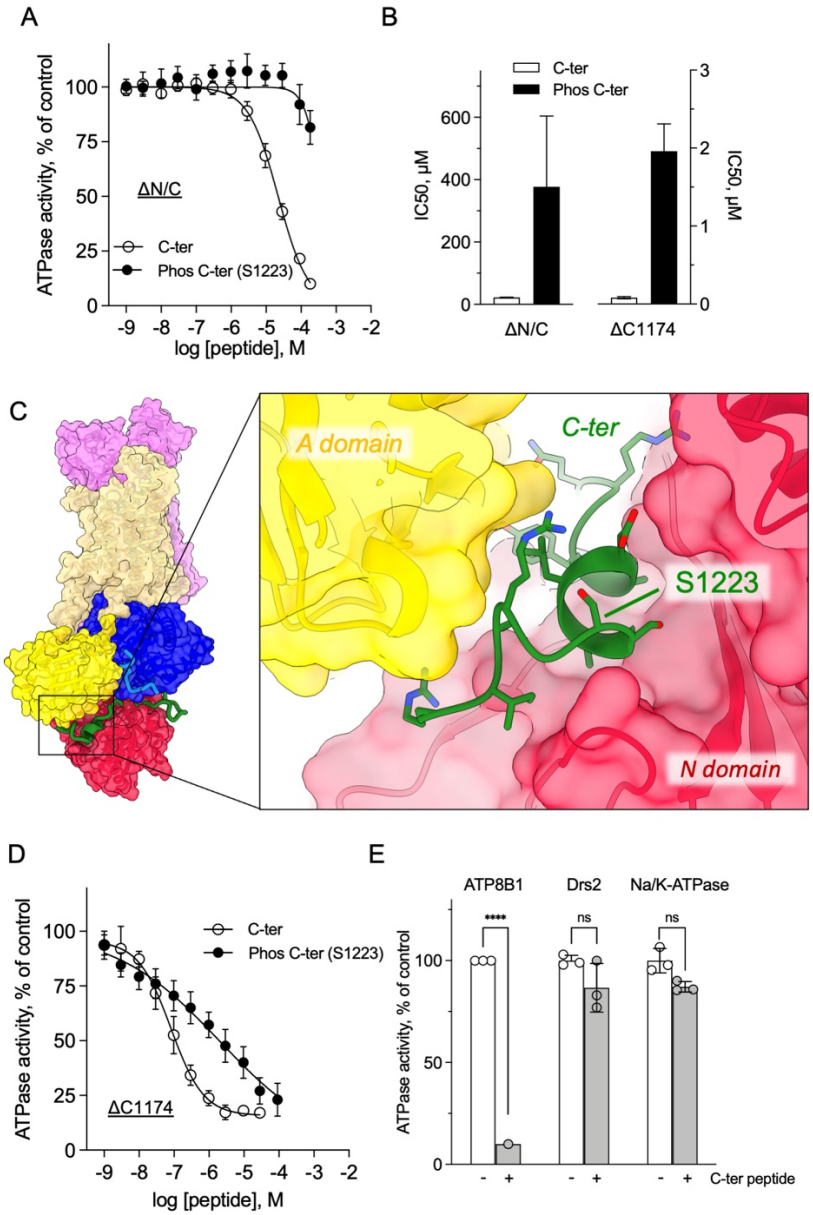

Figure 5 – Autoinhibition of ATP8B1 by its N- and C-terminal extensions.
(A) Back-inhibition of ΔN42/C1174 ATP8B1 (~ 3-3.3 μg ml^{-1} protein) by synthetic C-terminal peptides (C-ter, Phos C-ter). Activity was determined at 37°C. Data are mean ± s.d. of 3 replicate experiments. *(B)* Half-maximal inhibitory concentration (IC_{50}) of ATP8B1-CDC50A ATPase activity by C-terminal peptides deduced from curves in (*A*) and (*D*). Error bars represent the mean ± s.d. based on 33 to 47 data points. *(C)* Overall and close-up views of S1223 in the cleft formed by the A- and N-domains. The cytosolic A- and N-domains of ATP8B1 are colored in yellow and red, respectively, and are shown as surface and cartoon. The C-terminal tail of ATP8B1 is shown as cartoon with side chains in green. *(D)* Back-inhibition of ΔC1174 (~ 3-3.3 μg ml^{-1} protein) ATP8B1 by C-terminal peptides. Activity was determined at 37°C. For panels (*A*) and (*D*), the beryllium fluoride-sensitive ATPase activity is plotted as % of the activity in the absence of peptide. The data were fitted to an inhibitory dose-response equation with variable slope. Data are a mean ± s.d. of 3-4 replicate experiments. *(E)* Specificity of ATP8B1 inhibition by its C-terminal tail. ATPase activity of DDM-solubilized Drs2-Cdc50 (20 μg ml^{-1}) and pig α1β1 Na^+/K^+-ATPase (10 μg ml^{-1}) in microsomal membranes was determined at 30°C and 37°C, respectively, in the absence or presence of 180 μM ATP8B1 C-terminal peptide. The results shown in this panel for ATP8B1 inhibition are the same as those displayed in panel D for a concentration of 180 μM C-terminal peptide. **** $P < 0.0001$ according to two-way ANOVA with Tukey's test vs activity in the absence of peptide. ns: non significant. Data are a mean ± s.d. of 3 replicate experiments.

278

279 Large scale phosphoproteomic studies have shown that mouse ATP8B1 is phosphorylated at
280 residue S1223 (Huttlin et al., 2010; Villén et al., 2007). Given that S1223 is conserved between
281 mouse and human ATP8B1 and that this residue is located at the interface of the A- and the N-
282 domain (Fig. 5C), we used the C-terminal peptide to address the effect of this putative
283 phosphorylation on the autoinhibition mechanism. Remarkably, phosphorylation at S1223 impaired
284 the ability of the C-terminal peptide to inhibit ATP8B1, with an IC_{50} shifted to approximately 380 μM
285 (Fig. 5A and Fig. 5B). Furthermore, inhibition of ΔC1174 ATP8B1, i.e. still containing the N-terminal
286 tail, was about 270-fold more efficient (IC_{50} ~ 0.08 μM) than ΔN42/ΔC1174 (Fig. 5B and Fig. 5D).
287 Similar to the effect on the ΔN42/ΔC1174 variant, phosphorylation at S1223 decreased the ability of
288 the C-terminal peptide to inhibit ATPase activity of the ΔC1174 ATP8B1 variant (Fig. 5B and Fig.
289 5D). These results strongly support a prominent role for the N-terminal tail of ATP8B1 in the
290 autoinhibition mechanism. Importantly, inhibition was specific as neither the yeast P4-ATPase Drs2,
291 nor the cation-transporting Na^+/K^+-ATPase (a P2-ATPase), could be inhibited by the C-terminal tail
292 of ATP8B1 (Fig. 5E).
293 Together, our data reveal that the ATP8B1-CDC50A flippase is autoinhibited by its N- and C-terminal
294 extensions in a cooperative mechanism and that $PI(4,5)P_2$ is a major regulator of its activity.
295

296 **Lipid-dependence of ATP8B1 activity**

297 We showed that ATP8B1-CDC50A required PC and $PI(4,5)P_2$ for enzyme turnover (Fig. 4B). We
298 next explored the effect of other lipid species on the enzyme turnover in the presence of $PI(4,5)P_2$.
299 Under these conditions, PE and to a lesser extent PS, but not cardiolipin (CL) and sphingomyelin
300 (SM) could stimulate ATP8B1 activity (Fig. 6A). Plasma-membrane localized yeast P4-ATPases
301 Dnf1 and Dnf2 have been shown to transport lyso-phosphatidylcholine (Lyso-PC) (Riekhof et al.,
302 2007) and the alkylphosphocholine analogs miltefosine and edelfosine (Hanson et al., 2003), in
303 addition to PC (Pomorski et al., 2003). Furthermore, when co-expressed with CDC50A, murine
304 ATP8B1 was shown to increase uptake of the alkylphosphocholine analog perifosine in HeLa and
305 HEK293T cells (Muñoz-Martínez et al., 2010). As compared with background levels, Lyso-PC
306 induced a clear increase in the ATP hydrolysis rate of ATP8B1. Weak activation was also observed
307 in the presence of edelfosine and miltefosine (Fig. 6A).
308

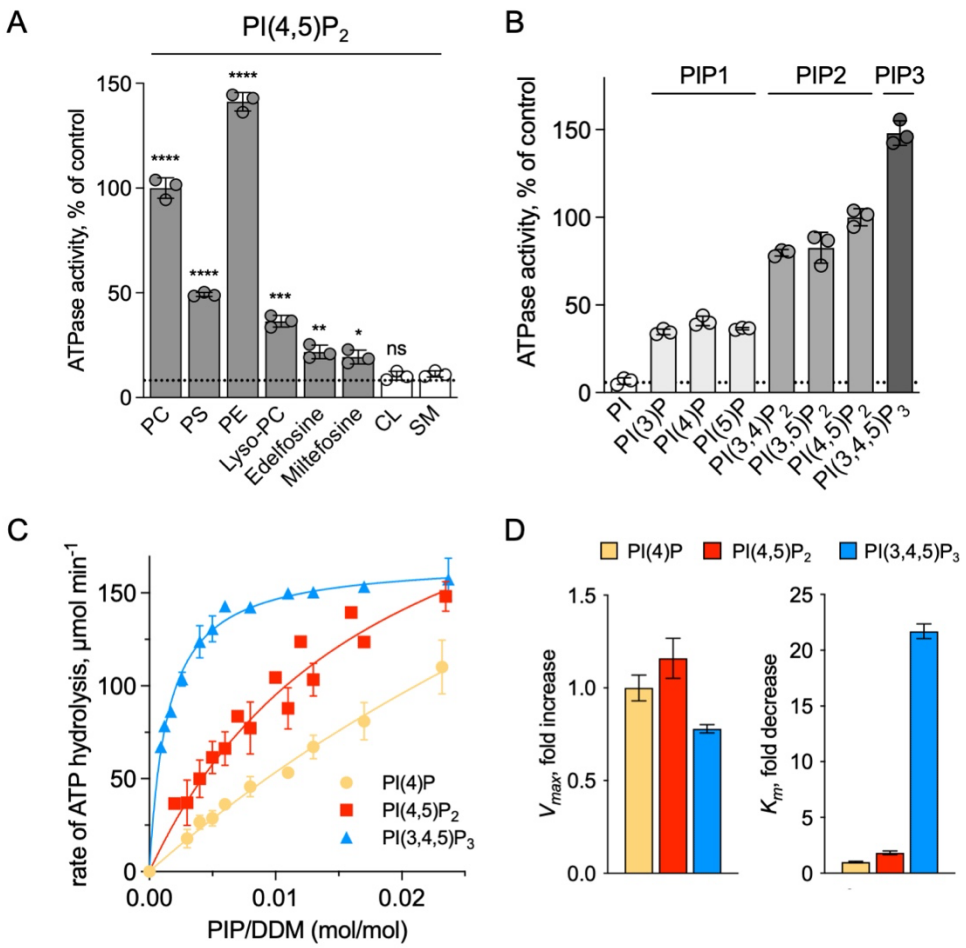

Figure 6 – Sensitivity of ATP8B1-CDC50A to phospholipids.
(A) ATPase activity of the ΔN42/C1174 ATP8B1 determined in the presence of various glycerophospholipids, lipid derivatives, and sphingomyelin. The specific activity measured in the presence of PC and PI(4,5)P_2 was taken as 100% (~0.15-0.3 μmol min^{-1} mg^{-1}). The dotted line represents the background activity measured in the absence of any added lipid. **** $P < 0.0001$, *** $P = 0.0002$, ** $P = 0.0071$, * $P = 0.0177$ according to unpaired two-tailed *t* test *vs* SM condition. ns: non significant. Data are mean ± s.d. of 3 replicate experiments. *(B)* ATPase activity of the ΔN42/C1174 ATP8B1 (0.5 μg ml^{-1}) determined in the presence of mono, di, and tri-phosphorylated phosphoinositides. In all cases, activity was measured in the presence of 2 mM DDM, 115 μM PC and 23 μM of the indicated phosphoinositides. The specific activity of the wild-type measured in the presence of PC and PI(4,5)P_2 was taken as 100%. The dotted line represents the activity measured in the sole presence of PC. Data are mean ± s.d. of 3 replicate experiments. *(C)* Apparent affinity of ΔN42/C1174 ATP8B1 (~ 3-3.3 μg ml^{-1}) for PI(4)P, PI(4,5)P_2 and PI(3,4,5)P_3. K_m for phosphoinositides was measured at 37°C in the presence of PC (POPC/DDM = 0.058 mol/mol). Plotted lines represent the best fit to a Michaelis-Menten equation. *(D)* Variations of the maximum velocity (V_{max}) and apparent affinity (K_m) of ΔN42/C1174 ATP8B1 for phosphoinositides calculated from double reciprocal plots displayed in Fig. S5, with respect to that measured in the presence of PI(4)P. The data in *(C)* and *(D)* represent the mean ± s.d. of 3-4 replicate experiments.

To further dissect the regulatory mechanism of ATP8B1-CDC50A, we examined the specificity of the purified enzyme for PPIns. All PPIn species were tested at the same molar concentration and at a fixed concentration of PC, and differed in the number and positions of phosphorylations on the

331 inositol headgroup. Phosphorylation of the headgroup appeared to be essential for stimulating
332 ATP8B1 ATPase activity, as no activity could be detected above background using
333 phosphatidylinositol (Fig. 6B). Monophosphorylated PPIn species, namely PI(3)P, PI(4)P, and
334 PI(5)P, were equally efficient in stimulating ATP hydrolysis by ATP8B1. When the inositol ring was
335 phosphorylated twice, the ATPase activity was increased about 2-fold compared to that observed
336 with monophosphorylated PPIns (Fig. 6B), with no dramatic difference in activity between PI(4,5)P_2,
337 PI(3,4)P_2, and PI(3,5)P_2. Tri-phosphorylated PI(3,4,5)P_3 increased further the activity of ATP8B1 by
338 about 1.5 fold. Thus, although the number of phosphorylations on the inositol ring matters, the
339 positions do not and ATP8B1-CDC50A can be activated by a wide variety of PPIns with increasing
340 efficiency linked to the number of phosphorylations. The differential activation by PPIns observed in
341 Fig. 6B could either be the result of a variation in the maximal velocity of ATP hydrolysis, the apparent
342 affinity for PPIns, or both. To distinguish between these possibilities, we measured the rate of ATP
343 hydrolysis by ATP8B1 in relation to the PPIn/detergent ratio (Fig. 6C), taking PI(4)P, PI(4,5)P_2 and
344 PI(3,4,5)P_3 as representative examples of singly, doubly and triply phosphorylated PPIns,
345 respectively. Whereas double-reciprocal plots indicated comparable maximum ATP hydrolysis rates
346 in the presence of PI(4)P, PI(4,5)P_2 and PI(3,4,5)P_3, the apparent affinity of ATP8B1 for PI(3,4,5)P_3
347 was found much higher than for PI(4)P and PI(4,5)P_2 (Fig. 6D and Fig. S5). Thus, ATP8B1 exhibits
348 a strong preference for PI(3,4,5)P_3 over other PPIns *in vitro*.
349

350 **Discussion**

351

352 Based on the cryo-EM structure of ATP8B1-CDC50A and dissection of its regulatory mechanism
353 using biochemical assays, we identify the C-terminal extension of ATP8B1 as a central component
354 in the regulation of its activity, and a cooperative contribution of the N-terminus of ATP8B1 in the
355 autoregulatory mechanism. Furthermore, we report that PPIns are essential activators of ATP8B1
356 activity and identify *in vitro* a preference for PI(3,4,5)P_3 in the activation of ATP8B1. Truncation of
357 the C- and N-termini of ATP8B1 allows switching ATP8B1 from a fully inhibited to an activated form,
358 provided lipid transport substrate and PPIns are present. Addition of a C-terminal peptide rescues
359 inhibition, and inhibition is subject to regulation by phosphorylation at S1223 of the C-terminal
360 extension.

361

362 **Autoinhibition of P4-ATPase flippases by their terminal tails: an evolutionarily conserved**
363 **mechanism? –** The autoinhibition of plasma membrane-localized ATP8B1 by its C-terminus is
364 reminiscent of that observed for the yeast endomembrane homolog Drs2. While an intact Drs2-
365 Cdc50 complex exhibits hardly any lipid-induced ATPase activity, once the C-terminus has been
366 trimmed off by proteases, the complex becomes competent for ATP hydrolysis (Azouaoui et al.,
367 2017). The ability of Drs2 to hydrolyze ATP requires not only displacement of its C-terminus but also
368 the binding of PI(4)P (Azouaoui et al., 2017; Timcenko et al., 2019). Cryo-EM structures show that
369 the C-terminus of Drs2 binds in a cleft between the P-domain and the N-domain, thus providing a
370 structural explanation for autoinhibition (Bai et al., 2019; Timcenko et al., 2019). The C-terminus also
371 appears to play a role in autoinhibition of ATP8A2, although this enzyme does not seem to be
372 regulated by PPIns (Chalat et al., 2017). In particular, the C-terminus of ATP8A1, a close relative of
373 ATP8A2, was recently shown to extend through its cytosolic catalytic domains (Hiraizumi et al., 2019;
374 Timcenko et al., 2019). This raises the question as to whether such autoregulatory mechanism is a
375 conserved feature among P4-ATPases. By comparing the sequences of P4-ATPase termini from
376 various organisms (Fig. 7 and Fig. S3 for a full alignment), it appears that although the C-termini of
377 P4-ATPases are in general poorly conserved, one exception to this rule is the ATP8B1 AYAFS motif
378 which occupies the ATP binding site. Furthermore, in the autoinhibited Drs2 and ATP8A1 structures,
379 their C-termini overlap extensively despite a rather low sequence conservation (Fig. 7). Noteworthy,
380 the C-terminal peptide of ATP8B1 did not exhibit an inhibitory effect on Drs2 (Fig. 5E), suggesting
381 that autoinhibition per se is mainly driven by the region downstream the conserved motif, the latter
382 mediating the interaction between the A and N domain. Thus, we predict that any P4-ATPase
383 containing the (G/A)(Y/F)AFS motif is likely to be autoinhibited by its C-terminus.

384

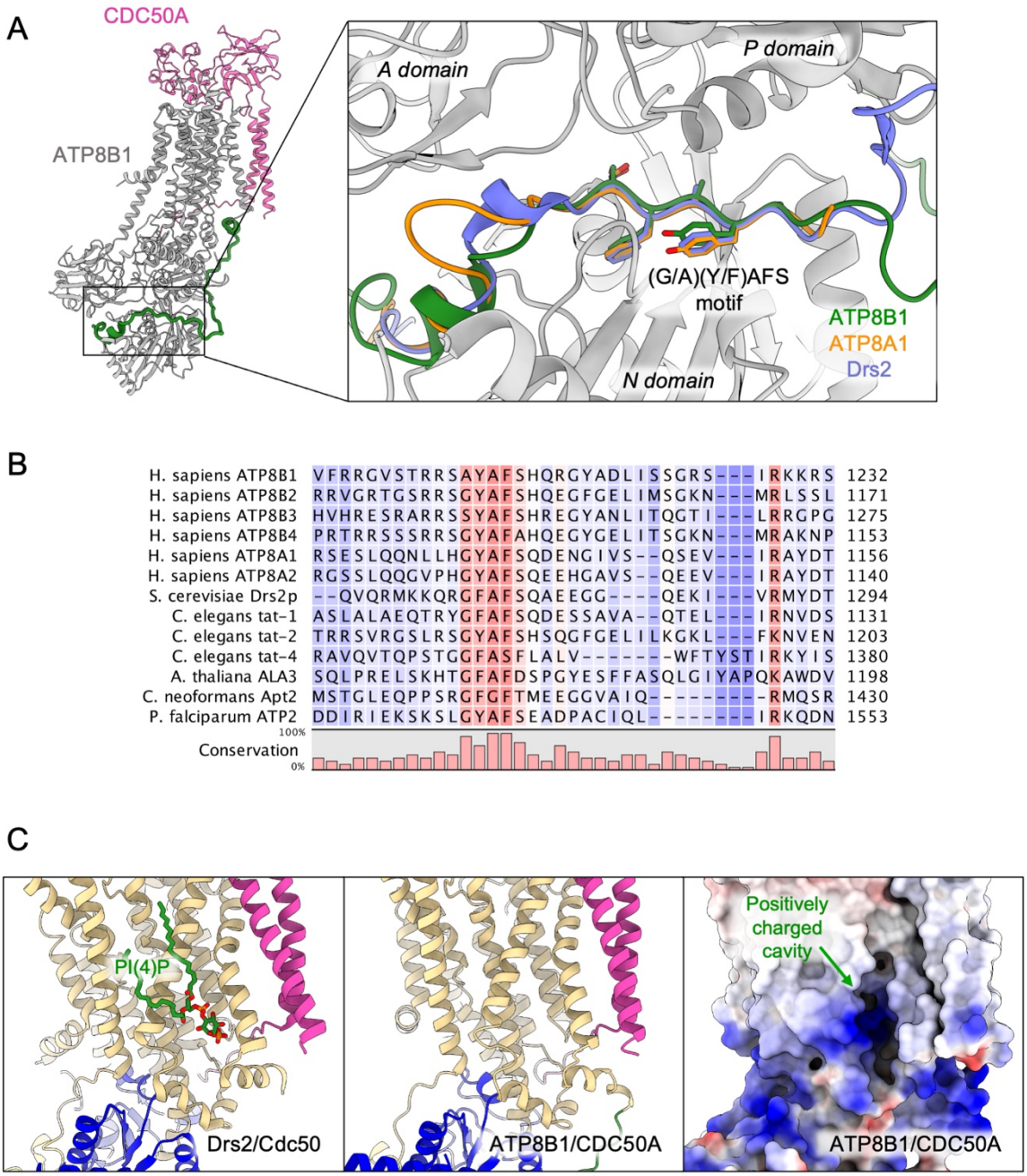

Figure 7 – Proposed mechanism for autoinhibition and regulation by phosphoinositides of the ATP8B1-CDC50A complex.

(A) Comparison of the binding sites of ATP8B1, ATP8A1 (PDB ID: 6K7N) and Drs2 (PDB ID: 6ROH) C-terminal tails, respectively in green, orange and blue reveals a common architecture and location of the inhibitory C-termini, and specifically the conserved (G/A)(Y/F)AFS motif (AYAFS for ATP8B1, GYAFS for ATP8A1 and GFAFS for Drs2) located in the ATP binding pocket. *(B)* Sequence alignment of select P4-ATPases C-termini, including ATP8B1, ATP8A1 and Drs2 which are all known to be autoinhibited. The shading indicates conservation (blue 0% – red 100%). *(C)* Side view of the PI(4)P-binding site of Drs2 (left). PI(4)P (in stick representation) is bound in the membrane domain. The same region in ATP8B1 reveals a similar organization (middle) with the presence of a positively-charged cavity (right) suggesting a putative phosphoinositide binding pocket in ATP8B1. CDC50A and Cdc50 transmembrane helices are colored in pink.

399

400 Our study also identifies a previously unrecognized role for the N-terminal tail of ATP8B1 in the
401 autoinhibition process. Although the precise mechanism is so far uncertain, our data indicate that
402 the N-terminal tail of ATP8B1 has a strong synergistic effect on the autoinhibition by its C-terminal
403 extension (Fig. 5D). Recent structures of Drs2, ATP11C and ATP8A1 have revealed a high degree
404 of flexibility of the cytosolic domains when the proteins are in the E1P state (Hiraizumi et al., 2019;
405 Nakanishi et al., 2020; Timcenko et al., 2021). The N-terminal tail might help to limit this flexibility via
406 its interaction with the A- and P-domains, as observed in our structure. Only the N-domain would
407 remain flexible, thereby facilitating C-terminus binding. A functional cooperation between N- and C-
408 termini has previously been described for the plant H^+-ATPase, a P-type ATPase from the P3
409 subfamily, where modifications in the N-terminus result in kinase-mediated phosphorylation in the
410 C-terminus, eventually leading to activation of the pump (Ekberg et al., 2010). Moreover, recent cryo-
411 EM structures revealed an autoinhibitory role for the N-terminus of the P5B-ATPase Ypk9 mediated
412 by its interaction with the cytosolic domains (Fig. S6), and it was proposed in this study that the C-
413 terminal tail of Ypk9 may also play a functional role owing to its interaction with the P-domain (Li et
414 al., 2021).
415

416 **Phosphorylation as a mechanism for the regulation of ATP8B1 activity –** The inhibitory
417 properties of a peptide derived from the C-terminus of ATP8B1 suggest that phosphorylation of
418 residue S1223 may provide additional regulation. Identification of the corresponding residue (S1223)
419 from the mouse orthologue ATP8B1 in large-scale phosphoproteomic studies (Huttlin et al., 2010;
420 Villén et al., 2007), suggests that phosphorylation of S1223 in human ATP8B1 might be part of the
421 autoinhibition relief mechanism *in vivo*. Consistent with this hypothesis, calcium/calmodulin-
422 dependent protein kinase II (CaMKII) has been shown to phosphorylate a serine residue, S1138, in
423 the autoinhibitory C-terminus of bovine ATP8A2. Substitution of S1138 to alanine resulted in a 33%
424 loss of the PS-dependent ATPase activity of ATP8A2 (Chalat et al., 2017). Interestingly, numerous
425 kinases, including PKC isoforms (Anwer, 2014), p38 mitogen-activated protein kinase (MAPK)
426 (Kubitz et al., 2004) and protein kinase A (PKA) have been linked to bile salt homeostasis (Gautherot
427 et al., 2012). More specifically, canalicular transporters also involved in inherited forms of
428 intrahepatic cholestasis such as the bile salt export pump (PFIC2, ABC11B) have been found
429 phosphorylated by PKC when overexpressed in insect cells (Noe et al., 2001) and the floppase
430 ABCB4 (PFIC3), known to transport PC in the opposite direction compared to ATP8B1, was shown
431 to be stimulated by PKA- and PKC-dependent phosphorylation (Gautherot et al., 2014). Future
432 studies are required to identify kinases responsible for the phosphorylation of S1223 and to

433 investigate the functional consequences of ATP8B1 phosphorylation on its activity, both *in vitro* and
434 in *vivo*.
435
436 **Regulation of ATP8B1-CDC50A by phosphoinositides** – In this study, we identified PPIns as
437 regulators of ATP8B1 ATPase activity. Whereas all PPIns showed the ability to stimulate ATP8B1
438 activity (Fig. 6), PI(3,4,5)P_3 displayed a much higher affinity for ATP8B1 than other PPIns.
439 PI(3,4,5)P_3 is primarily localized at the plasma membrane, and one of the least abundant PPIns in
440 mammalian cells, being virtually undetectable in quiescent cells. However, upon activation of cell-
441 surface receptors and recruitment of class I PI3-kinases, PI(3,4,5)P_3 levels may rise up to 50-fold,
442 albeit at levels that are 10% lower than cellular PI(4,5)P_2 (Clark et al., 2011). The tight control of
443 PI(3,4,5)P_3 concentration stems from its critical role in key signaling pathways such as cell
444 proliferation, survival and membrane trafficking (Marat and Haucke, 2016). The lower K_m of ATP8B1
445 for PI(3,4,5)P_3 than for other PPIns suggests that the cavity where PI(3,4,5)P_3 binds is specifically
446 adjusted to this PPIn, whereas other PPIns can fit as well, but less efficiently. To our knowledge,
447 direct regulation of integral membrane proteins by PI(3,4,5)P_3 has not previously been shown.
448 Intriguingly, despite addition of PI(3,4,5)P_3 during sample preparation for cryo-EM studies, no clear
449 density could be observed for this lipid. However, the cavity lined by TM7, TM8 and TM10 on the
450 structure of ATP8B1, which corresponds to the PI(4)P binding site in Drs2, consists of a large number
451 of basic residues (Fig. 7) strongly hinting at a similar site in both Drs2 and ATP8B1. It is possible
452 that PPIns can bind only once autoinhibition is relieved, at variance with Drs2 where PI(4)P has been
453 shown to be important in the relief of autoinhibition.
454 Irrespective of this, the physiologically relevant regulatory PPIn is still unknown. Given the
455 localization of ATP8B1 in the apical membrane of epithelial cells in mammals, and the subcellular
456 localization and abundance of PPIns in cell membranes (Balla, 2013; Dickson and Hille, 2019), both
457 PI(3,4,5)P_3 and PI(4,5)P_2 might fulfill this task. Future studies aimed at manipulating PPIns levels in
458 living cells should help reveal whether ATP8B1 depends on specific PPIns *in vivo*.
459
460 **Structural basis for catalytic deficiency induced by inherited ATP8B1 mutations** – Our
461 structural model of ATP8B1 enabled us to map the mutations found in patients suffering from PFIC1,
462 BRIC1 or ICP1 (Bull et al., 1998; Deng et al., 2012; Dixon et al., 2017; Klomp et al., 2004; Painter et
463 al., 2005) (Fig. 8A). Mutations are homogenously distributed along the protein sequence, and some
464 mutations are likely to impair catalytic properties of ATP8B1 directly (Fig. 8B). Mutations D554N and
465 H535L are located in the nucleotide binding pocket, suggesting that these mutations might prevent
466 or affect ATP binding. The D554 residue is at interacting distance with the autoinhibitory C-terminus
467 and its mutation might also strengthen autoregulation. Additionally, mutations S453Y, D454G and

468 T456M in the P-domain will abolish autophosphorylation of the catalytic aspartate (D454), thus
469 resulting in an inactive ATP8B1.
470

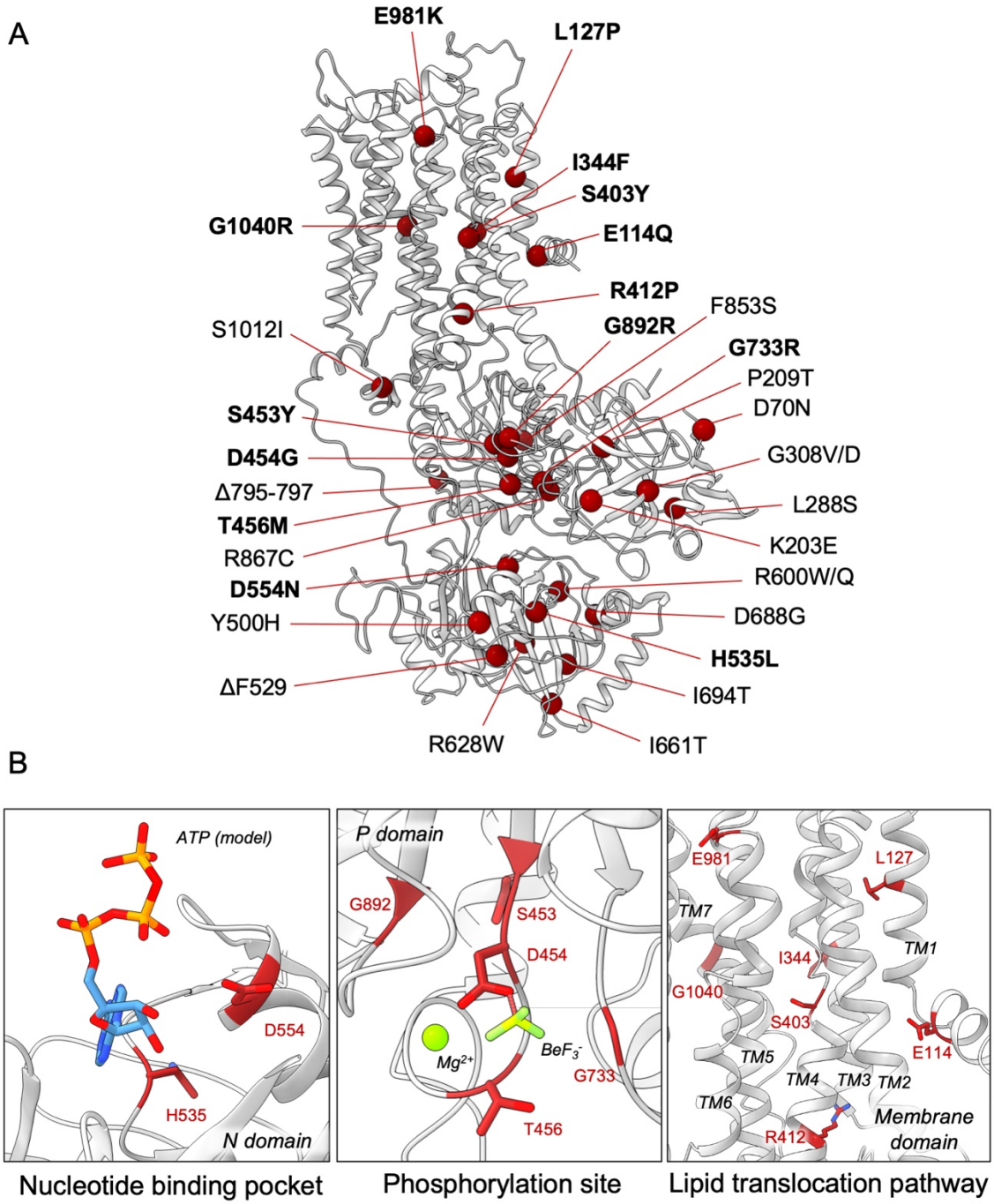

471

472 **Figure 8 – Structural map of the inherited intrahepatic disease-related mutations.**
473 (*A*) Mutations found in PFIC1, BRIC1 or ICP1 patients are shown as red spheres on ATP8B1 $E2P_{autoinhibited}$
474 structure (in grey). Mutations indicated in bold are presented in panel *(B). (B)* Close-up views of the nucleotide
475 binding site within the N-domain of ATP8B1. The ATP molecule position was model by aligning ATP8B1 N
476 domain with the N domain of ATP8A1 in E1-ATP bound state (PDB: 6K7J) (left). (Middle) the phosphorylation
477 site in the P-domain with Mg^{2+} and the phosphate mimic BeF_3^- in green. (Right) the lipid transport pathway.
478
479

480

481 The structure of ATP8B1 presented in this report is locked in a $E2P_{autoinhibited}$ state where the
482 exoplasmic lipid pathway is closed (Timcenko et al., 2019). However, it is important to note that
483 numerous mutations can be found in this region (Fig. 8B). The S403 residue, mutated to a tyrosine
484 in PFIC1, is part of the PISL motif conserved in P4-ATPases. The PISL motif is located in TM4 and
485 has been shown to interact with the phosphoglycerol backbone of PS, the transport substrate of
486 Drs2 and ATP8A1 (Hiraizumi et al., 2019; Timcenko et al., 2019). A relatively conservative mutation
487 of this Ser into Ala in ATP8A2 (S365A), has been shown to significantly diminish its ATPase activity
488 and transport substrate affinity (Vestergaard et al., 2014). Moreover, mutations E981K and L127P
489 have also been shown to impair ATP8B1-catalyzed transport of PC *in vivo* (Takatsu et al., 2014).
490 Mutation of the corresponding residues in the PS-specific ATP8A2 alters ATPase activity and lipid
491 specificity (Gantzel et al., 2017). Further functional and structural studies will be needed to better
492 understand how these mutations may affect substrate recognition and translocation.
493

494 **Conclusions –** Our findings show that the plasma membrane P4-ATPase ATP8B1 is tightly
495 regulated by its N- and C-terminal tails as well as PPIns and that the autoinhibitory mechanism can
496 be mimicked by exogenous peptides. Understanding the regulatory mechanism of mammalian P4-
497 ATPases will be instrumental for the subsequent design of molecules that would enforce/mimic or
498 stimulate the release of the autoinhibitory C-terminus. We propose that the regulatory mechanism
499 uncovered in this study may be a feature shared by other P4-ATPases, and by analogy with the
500 yeast endomembrane flippase Drs2, that associated proteins are likely to be involved in the
501 regulation of ATP8B1 activity. Moreover, these studies will pave the way towards detailed functional
502 assessment of disease-associated ATP8B1 mutations found in PFIC1 patients.
503

504 **Materials and Methods**

505

506 **Materials**

507 Products for yeast and bacteria cultures were from Difco (BD Biosciences) and Sigma. DNA
508 Polymerase, restriction and modification enzymes, as well as Endoglycosidase H-MBP, were
509 purchased from New England Biolabs (NEB). Lauryl Maltose Neopentyl Glycol (LMNG, NG310) and
510 *n*-dodecyl-β-D-maltopyranoside (DDM, D310) were from Anatrace, cholesteryl hemisuccinate (CHS)
511 from Sigma (C6013). Brain phosphatidylinositol-4-phosphate (PI(4)P), brain phosphatidylinositol-
512 4,5-bisphosphate (PI(4,5)P_2), 1,2-dioleoyl-*sn*-glycero-3-phospho-(1'-myo-inositol-3'-phosphate)
513 (PI(3)P), 1,2-dioleoyl-*sn*-glycero-3-phospho-(1'-myo-inositol-5'-phosphate) (PI(5)P), 1,2-dioleoyl-*sn*-
514 glycero-3-phospho-(1'-myo-inositol-3',4'-bisphosphate) (PI(3,4)P_2), 1,2-dioleoyl-*sn*-glycero-3-
515 phospho-(1'-myo-inositol-3',5'-bisphosphate) (PI(3,5)P_2) and 1,2-dioleoyl-*sn*-glycero-3-phospho-(1'-
516 myo-inositol-3',4',5'-trisphosphate) (PI(3,4,5)P_3) were from Avanti Polar lipids. Brain PS, 1-palmitoyl-
517 2-oleoyl-*sn*-glycero-3-phosphocholine (POPC), 1-palmitoyl-2-oleoyl-*sn*-glycero-3-
518 phosphoethanolamine (POPE), 1-palmitoyl-2-oleoyl-*sn*-glycero-3-phosphoserine (POPS), heart
519 cardiolipin (CL), egg sphingomyelin (SM) and edelfosine were also from Avanti Polar lipids.
520 Miltefosine (also known as Fos-choline-16, FC-16) was from Anatrace (F316) and 1-stearoyl-2-
521 hydroxy-sn-glycero-3-phosphocholine (Lyso-PC) was from Sigma. The ATP8B1 C-terminal peptide
522 RRSAYAFSHQRGYADLISSGRSIRKKRSPLDAIVADGTAEYRRTGDS, encompassing residues
523 1205-1251, and its S1223 phosphorylated derivative, were ordered from Biomatik Company
524 (Biomatik, Ontario, Canada). Both peptides were resuspended at 1 mM in 50 mM MOPS-Tris pH 7,
525 100 mM KCl, 1 mM dithiothreitol (DTT). ATP8B1 was detected using a mouse anti-ATP8B1 antibody
526 from Santa Cruz Biotechnology (Epitope: 1161-1251, ref: SC-134967, no longer available). An anti-
527 mouse HRP-coupled antibody (1706516) was from Biorad. His-tagged CDC50A was detected using
528 a His-probe™ -HRP from Thermo Scientific (15165). Precast stain-free gradient gels for tryptophan
529 fluorescence (4568084) as well as Precision Plus Protein Standards (1610393) were from Biorad.
530 Pyruvate kinase (P7768), lactate dehydrogenase (L1006), and an EDTA-free protease inhibitor
531 cocktail (S8830) were from Sigma. [γ-^{32}P]ATP was purchased from Perkin-Elmer (BLU002A).
532 Streptavidin-sepharose resin was from GE/Cytiva (17511301).
533 The pig kidney α1β1 isoform of Na^+/K^+-ATPase was a kind gift from Mads Eskesen Christensen and
534 microsomal membranes were prepared as previously described (Klodos et al., 2002).

535

536 **Yeast strains and plasmids**

537 The *Saccharomyces cerevisiae* W303.1b/*Δpep4* (*MATα, leu2-3, his3-11, ura3-1, ade2-1, Δpep4,*
538 *can^r, cir$^+$*) yeast strain was used for co-expression of ATP8B1 and CDC50A. The cDNAs encoding

539 human ATP8B1 (hATP8B1, Uniprot: O43520; A1154T natural variant) and human CDC50A
540 (hCDC50A, Uniprot: Q9NV96) were a kind gift from Joost Holthuis (University of Osnabruck,
541 Germany). hATP8B1 was supplemented at its 5' end with a sequence coding a biotin acceptor
542 domain (BAD), and a sequence coding a TEV protease cleavage site. The cleavage site was flanked
543 by 2 glycines toward BAD and 4 glycines toward hATP8B1. Similarly, a sequence coding a
544 decahistidine tag was added at the 5' end of hCDC50A. The tagged genes were cloned in a unique
545 co-expression pYeDP60 plasmid (Jacquot et al., 2012). In this vector, hATP8B1 and hCDC50A are
546 both placed under the control of a strong galactose-inducible promoter, *GAL10/CYC1*. The D454N
547 mutation was introduced by site-directed mutagenesis using the QuickChange™ II XL site-directed
548 mutagenesis kit (Agilent technologies). An overlap extension PCR strategy was used to insert the
549 3C protease site (LEVLFQGP) between Pro42 and Glu43 and/or between Glu1174 and Ser1175.
550
551 **Co-expression of ATP8B1 with CDC50A in yeast membranes**
552 Yeasts were transformed using the lithium-acetate method (68). Yeast cultures, recombinant protein
553 expression and membrane preparation were performed as described previously (45, 69). Briefly,
554 yeast growth took place in a glucose-containing rich growth medium supplemented with 2.7%
555 ethanol at 28°C for 36 h, whereas expression of the proteins of interest took place during an
556 additional 18 h in the presence of 2% galactose, at 18°C. Yeast cells were harvested by
557 centrifugation, washed first with ice-cold ddH_2O, then with ice-cold TEKS buffer (50 mM Tris-HCl pH
558 7.5, 1 mM EDTA, 0.1 M KCl, 0.6 M sorbitol), and finally resupended in TES buffer (50 mM Tris-HCl
559 pH 7.5, 1 mM EDTA, 0.6 M sorbitol) supplemented with protease inhibitors. The cells were
560 subsequently broken with 0.5 mm glass beads using a "Pulverisette 6" planetary mill (Fritsch). The
561 crude extract was then spun down at 1,000 *g* for 20 min at 4°C, to remove cell debris and nuclei.
562 The resulting supernatant was centrifuged at 20,000 *g* for 20 min at 4°C, yielding S2 supernatant
563 and P2 pellet. The S2 supernatant was further centrifuged at 125,000 *g* for 1 h at 4°C. The resulting
564 P2 and P3 pellets were finally resuspended at about 30-50 mg ml^{-1} of total protein in TES buffer. P2
565 and P3 membrane fractions were pooled and the ATP8B1 content was estimated, by
566 immunoblotting, to be about 0.5% of total proteins.
567
568 **Purification of the ATP8B1-CDC50A complex**
569 Membranes obtained after co-expression of ATP8B1 and CDC50A (P2+P3) were diluted to 5 mg ml^{-1}
570 of total protein in ice-cold buffer A (50 mM MOPS-Tris at pH 7, 100 mM NaCl, 1 mM DTT, 20%
571 (w/v) glycerol and 5 mM $MgCl_2$), supplemented with 1 mM PMSF and an EDTA-free protease
572 inhibitor mixture. The suspension was stirred gently on a wheel for 5 min at 4°C. Washed membranes
573 were pelleted by centrifugation at 100,000 *g* for 1 h at 4°C. For cryo-EM sample preparation, this

574 step was omitted and the membranes were directly incubated with DDM as follows. The pelleted
575 membranes were resuspended at 5 mg ml^{-1} of total protein in ice-cold buffer A supplemented with 1
576 mM PMSF and the EDTA-free protease inhibitor mixture. A mixture of DDM and CHS at final
577 concentrations of 15 mg ml^{-1} and 3 mg ml^{-1}, respectively, was added, resulting in a DDM/protein ratio
578 of 3/1 (w/w). The suspension was then stirred gently on a wheel for 1 h at 4°C. Insoluble material
579 was pelleted by centrifugation at 100,000 *g* for 1 h at 4°C. The supernatant, containing solubilized
580 proteins, was applied onto a streptavidin-sepharose resin and incubated for 2 h at 6°C to allow
581 binding of the BAD-tagged ATP8B1 to the resin.
582 For structural studies the DDM/CHS mixture was exchange to LMNG/CHS. The resin was washed
583 twice with three resin volumes of ice-cold buffer B (50 mM MOPS-Tris at pH 7, 100 mM KCl, 1 mM
584 DTT, 20% (w/v) glycerol and 5 mM $MgCl_2$), supplemented with 0.2 mg ml^{-1} LMNG and 0.02 mg ml^{-1}
585 CHS in the presence of 1 mM PMSF and an EDTA-free protease inhibitor cocktail. The resin was
586 then washed thrice with three resin volumes of ice-cold buffer B supplemented with 0.1 mg ml^{-1}
587 LMNG and 0.01 mg ml^{-1} CHS. Elution was performed by addition of 60 μg of purified TEV per ml of
588 resin and overnight incubation at 6°C. The eluted fraction was concentrated using a Vivaspin unit
589 (100 kDa MWCO) prior to injection on a size-exclusion Superose 6 10/300GL increase column
590 equilibrated with buffer C (50 mM MOPS-Tris pH 7, 100 mM KCl, 1 mM DTT, 5 mM $MgCl_2$, 0.03 mg
591 ml^{-1} LMNG and 0.003 mg ml^{-1} CHS). The ATP8B1-CDC50A-containing fractions were pooled,
592 concentrated using a Vivaspin unit (50 kDa MWCO) to concentrate the protein and the detergent
593 micelles, and supplemented with LMNG and $PI(3,4,5)P_3$ to final concentrations of 0.35 mg ml^{-1} and
594 0.05 mg ml^{-1}, respectively ($PI(3,4,5)P_3$/LMNG ratio of 0.15). The sample was then incubated for 1 h
595 at room temperature and overnight at 6°C to allow lipid diffusion prior injection on a Superose 6
596 10/300GL increase column equilibrated with buffer C, to remove the excess of detergent/lipid
597 micelles.
598 For functional studies, the resin was washed four times with three resin volumes of ice-cold buffer B
599 supplemented with 0.5 mg ml^{-1} DDM and 0.1 mg ml^{-1} CHS in the presence of 1 mM PMSF and an
600 EDTA-free protease inhibitor cocktail. Elution was performed by addition of 60 μg of purified TEV
601 per mL of resin by overnight incubation at 6°C. For purifying the 3C protease site-containing version
602 of ATP8B1, 240 μg of purified 3C protease per ml of resin were added together with the TEV
603 protease. Purified ATP8B1-CDC50A complex was snap-frozen and stored at -80°C. ATP8B1 protein
604 concentrations were calculated based on Coomassie-blue staining of SDS-PAGE gels using known
605 amounts of purified Drs2.
606
607 **Grid preparation for cryo-EM**

608 The ATP8B1-CDC50A complex at a concentration of 0.8 mg ml^{-1} was supplemented with 1 mM
609 $BeSO_4$ and 5 mM KF to obtain the E2P conformation. The sample was incubated on ice for 1 h and
610 3 μl were added to freshly glow-discharged (45 seconds at 15 mA) C-flat Holey Carbon grids, CF-
611 1.2/1.3-4C (Protochips), which were subsequently vitrified at 4°C and 100% humidity on a Vitrobot
612 IV (Thermo Fisher Scientific).
613
614 **Cryo-EM data collection**
615 The Data were collected on a Titan Krios G3i (EMBION Danish National cryo-EM Facility – Aarhus
616 node) with X-FEG operated at 300 kV and equipped with a Gatan K3 camera and a Bioquantum
617 energy filter using a slit width of 20 eV and with 30° tilt. Movies were collected using aberration-free
618 image shift data collection (AFIS) in EPU (Thermo Fisher Scientific) as 1.5 second exposures in
619 super-resolution mode at a physical pixel size of 0.66 Å/pixel (magnification of 130,000x) with a total
620 electron dose of 60e-/Å2. A total of 3941 movies were collected.
621
622 **Cryo-EM data processing**
623 Processing was performed in cryoSPARC v3 (Punjani et al., 2017). Patch Motion Correction and
624 Patch CTF were performed before low-quality micrographs (e.g. micrographs with crystalline ice,
625 high motion) were discarded. Particles were initially picked using a circular blob on ~1000
626 micrographs. These were aligned in 2D to produce references for template picking on all movies.
627 Particles were extracted in a 416-pixel box and Fourier cropped to a 104-pixel box (2.64 Å/pixel). *Ab*
628 *initio* references were produced using a subset of all particles. One protein-like reference and
629 multiple junk references were used in multiple rounds of heterogeneous refinement. Selected
630 particles were then re-extracted in a 416-pixel box (0.66 Å/pixel) before non-uniform (NU) refinement
631 (Punjani et al., 2020). The particle stack was then CTF-refined using Local CTF refinement and
632 motion-corrected using Local motion correction before final non-uniform (NU) refinement. Data
633 processing flow-chart is available in Fig. S7.
634
635 **Model building**
636 The ATP8B1-CDC50A model was built using a homology model of ATP8B1 generated by I-TASSER
637 (Yang et al., 2015) with Drs2 $E2P_{autoinhibited}$ (PDB: 6ROH) and from the CDC50A structure of the
638 ATP8A1-CDC50A complex in E2P (PDB: 6K7L) as templates. The cryo-EM map was sharpened
639 with a B factor of -84 $Å^2$ using the Autosharpen tool in PHENIX (Terwilliger et al., 2018).
640 The model was manually generated and relevant ligands added with COOT (Emsley et al., 2010)
641 before real space refinement in PHENIX (Afonine et al., 2018) with secondary structure restraints.
642 Model validation was performed using MolProbity (Chen et al., 2010) in PHENIX (Pd et al., 2010),

643 and relevant metrics are listed in Table S1. Representative map densities with fitted models can be
644 seen in Fig. S2. Figures were prepared in ChimeraX (Pettersen et al., 2021).
645
646 **Endoglycosidase treatment**
647 For CDC50A deglycosylation, the purified sample was treated with EndoH-MBP according to
648 manufacturer instructions. Briefly, about 1.5 *µ*g of purified ATP8B1-CDC50A complex was
649 denatured for 3 min at 96°C in the presence of 0.5% SDS and 40 mM DTT, in a final volume of 19.5
650 *µ*l. The denatured proteins were then supplemented with 500 U of EndoH-MBP (EndoHf, NEB) and
651 incubated 45 min at 37°C. Then 20 *µ*l of urea-containing Laemmli denaturation buffer were added
652 and the samples were incubated for 10 min at 30°C prior loading on an 8% SDS-PAGE.
653
654 **Determination of subunit stoichiometry**
655 About 6.5 *µ*g of purified ATP8B1-CDC50A complex was denatured for 5 min at 96°C, in presence of
656 0.5% SDS and 40 mM DTT and in a final volume of 250 *µ*l. The denatured proteins were then
657 supplemented with 750 U of EndoH-MBP and incubated for 1 h at 37°C Samples were then
658 precipitated by adding 1 volume of 1 M trichloroacetic acid (TCA). After 45 min on ice, samples were
659 centrifuged at 20,000 *g* for 25 min at 4°C. Supernatant was discarded and samples were centrifuged
660 again at 20,000 *g* for 5 min at 4°C to remove traces of TCA. Pellets were then resuspended in 60 *µ*l
661 urea-containing Laemmli buffer (50 mM Tris-HCl pH 6.8, 0.7 M β-mercaptoethanol, 2.5% w/v SDS,
662 0.5 mM EDTA, 4.5 M urea, 0.005% w/v bromophenol blue). Thirty *µ*l of each sample (about 3.25 *µ*g
663 of purified complex) were loaded on a 4-15% gradient TGX™ stain-free gel. After 90 min
664 electrophoretic separation at 150 V and 40 mA, the gel was soaked in 5% (w/v) TCA for 10 min. The
665 gel was then rinsed 3 times in ddH_2O. The gel was then exposed to UV (254 nm) for 5 min and
666 images were collected after 20 s of exposure. The relative intensity of ATP8B1 and CDC50A was
667 quantified from various amounts loaded onto gradient TGX™ stain-free gels using the ImageJ
668 software.
669
670 **Phosphorylation of ATP8B1-CDC50A by [γ-^{32}P]ATP**
671 To study phosphorylation of the ATP8B1/CDC50A complex, about 0.5 *µ*g of purified complex were
672 supplemented with [γ-^{32}P]ATP at a final concentration of 2 *µ*M (5 mCi *µ*mol^{-1}) and incubated at 0°C
673 in buffer B supplemented with 0.5 mg ml^{-1} DDM and 0.1 mg ml^{-1} CHS. Phosphorylation was stopped
674 after 30 sec by addition of 1 sample volume of 1 M TCA, 5 mM H_3PO_4. Samples were then left for
675 40 min on ice for aggregation and 2 volumes of 0.5 M TCA in 2.5 mM H_3PO_4 were subsequently
676 added to help aggregation. Proteins were then centrifuged at 14,000 *g* for 25 min at 4°C. The
677 supernatant was removed, and the pellet was washed by addition of 0.5 M TCA in 0.5 mM H_3PO_4.

678 Samples were centrifuged again at 14,000 *g* for 25 min at 4°C. Supernatants were discarded,
679 samples were centrifuged again at 14,000 *g* for 5 min at 4°C to remove residual TCA. Pellets were
680 then resuspended at 4°C in 25 μl urea-containing Laemmli denaturation buffer. After resuspension,
681 15 μl of each sample (about 0.3 μg of purified complex) were loaded on acidic gels. The stacking
682 gel contained 4% acrylamide, 65 mM Tris-H_3PO_4 pH 5.5, 0.1% SDS, 0.4% ammonium persulfate,
683 and 0.2% TEMED, and the separating gel was a continuous 7% gel containing 65 mM Tris-H_3PO_4
684 pH 6.5, 0.1% SDS, 0.4% ammonium persulfate, and 0.05% TEMED. The gel tanks were immersed
685 in a water/ice bath and the pre-cooled running buffer contained 0.1% SDS and 170 mM MOPS-Tris
686 at pH 6.0. Dried gels were subsequently stained with Coomassie Blue before radioactivity was
687 measured, using a PhosphorImager equipment (Amersham Typhoon RGB, GE Healthcare).
688
689 **ATPase activity of purified ATP8B1-CDC50A**
690 For the ATP8B1-CDC50A complex, the rate of ATP hydrolysis was monitored continuously using an
691 enzyme-coupled assay, via its coupling to a drop of NADH absorption at 340 nm. ATPase activity
692 was measured at either 30°C or 37°C in buffer B supplemented with 1 mM ATP, 1 mM
693 phosphoenolpyruvate, 0.4 mg ml^{-1} pyruvate kinase, 0.1 mg ml^{-1} lactate dehydrogenase, 250 μM
694 NADH, 1 mM NaN_3, 1 mg ml^{-1} DDM (2 mM), and residual CHS at 0.01 mg ml^{-1}. In these experiments,
695 50-200 μl of the purified ATP8B1-CDC50A complex (final concentrations of 1-5 μg ml^{-1}) in the various
696 experiments, was added to a total volume of 1.8 ml. For measurement of the half-maximum inhibitory
697 concentration (IC_{50}), successive additions of the C-terminal peptide or its phosphorylated derivative
698 (from a 1 mM stock solution) to purified ATP8B1-CDC50A incubated in 43 μg ml^{-1} POPC (~ 57 μM),
699 25 μg ml^{-1} PI(4,5)P_2 (~ 23 μM) and 0.5 mg ml^{-1} DDM (~ 1 mM) in the assay cuvette were performed.
700 Similarly, to determine the maximum rate of ATP hydrolysis (V_{max}) and the apparent affinity (K_m) for
701 PPIns, successive additions of DDM and POPC to purified ATP8B1-CDC50A preincubated with 43
702 μg ml^{-1} POPC, 25 μg ml^{-1} PI(4,5)P_2 and 0.5 mg ml^{-1} DDM were performed, in order to gradually
703 decrease the PIP/DDM ratio (while the POPC/DDM ratio remained constant). Conversion from
704 NADH oxidation rates expressed in mAU s^{-1} to ATPase activities expressed in μmol min^{-1} mg^{-1} was
705 based on the extinction coefficient of NADH at 340 nm (~ 6.2 mM^{-1} cm^{-1}). For all experiments,
706 photobleaching of NADH was reduced by inserting an MTO J310A filter that eliminates short
707 wavelength UV exciting light. This setup reduced the spontaneous rate of NADH absorption changes
708 down to ~ 0.01 mAU s^{-1}.
709

Acknowledgments

We thank Thomas Boesen, Andreas Bøggild and Taner Drace for technical support during EM data collection at the EMBION Cryo-EM facility of Aarhus University, Jesper Lykkegaard Karlsen for scientific computing support, Joost Holthuis (University of Osnabruck, Germany) for kindly providing the ATP8B1 and CDC50A cDNAs, Rosa López-Marqués (University of Copenhagen, Denmark) for the gift of the *S. cerevisiae Δpep4* strain and Mads Eriksen Christensen and Natalya Fedosova for generously providing the pig kidney α1β1 isoform of Na^+/K^+-ATPase. We also wish to thank David Stokes for critical reading of the manuscript and Philippe Champeil, Alenka Čopič, Guillaume Drin, Rasmus Kock Flygaard, Francis Haraux, Anaïs Lamy, José Luis Vázquez-Ibar and Marc le Maire for discussion and advice. Support for this work was provided by an ANR grant (ANR-14-CE09-0022) to G.L., by an EMBO short-term fellowship (7881), a PhD fellowship from the French ministry for higher education, research and innovation, and a Marie-Curie Individual Fellowship (LivFlip, grant agreement 101024542, H2020-MSCA-IF-2020) to T.D., by the French Infrastructure for Integrated Structural Biology (FRISBI; ANR-10-INSB-05), by the Centre National de la Recherche Scientifique (CNRS), by a professorship grant from the Lundbeck Foundation (R310-2018-3713) and by the German Research Foundation (GU 1133/11-1).

Data availability

The ATP8B1-CDC50A $E2P_{autoinhibited}$ cryo-EM map described in this article has been deposited in the Electron Microscopy Data Bank (EMDB) (accession number: EMD-13711) and atomic models have been deposited in the Protein Data Bank (PDB) (accession number: 7PY4).

References

Afonine PV, Poon BK, Read RJ, Sobolev OV, Terwilliger TC, Urzhumtsev A, Adams PD. 2018. Real-space refinement in PHENIX for cryo-EM and crystallography. *Acta Crystallogr Sect Struct Biol* **74**:531–544. doi:10.1107/S2059798318006551

Albers RW. 1967. Biochemical aspects of active transport. *Annu Rev Biochem* **36**:727–756. doi:10.1146/annurev.bi.36.070167.003455

Andersen JP, Vestergaard AL, Mikkelsen SA, Mogensen LS, Chalat M, Molday RS. 2016. P4-ATPases as Phospholipid Flippases-Structure, Function, and Enigmas. *Front Physiol* **7**:275. doi:10.3389/fphys.2016.00275

Anwer MS. 2014. Role of protein kinase C isoforms in bile formation and cholestasis. *Hepatol Baltim Md* **60**:1090–1097. doi:10.1002/hep.27088

Azouaoui H, Montigny C, Dieudonné T, Champeil P, Jacquot A, Vázquez-Ibar JL, Le Maréchal P, Ulstrup J, Ash M-R, Lyons JA, Nissen P, Lenoir G. 2017. High phosphatidylinositol 4-phosphate (PI4P)-dependent ATPase activity for the Drs2p-Cdc50p flippase after removal of its N- and C-terminal extensions. *J Biol Chem* **292**:7954–7970. doi:10.1074/jbc.M116.751487

Bai L, Kovach A, You Q, Hsu H-C, Zhao G, Li H. 2019. Autoinhibition and activation mechanisms of the eukaryotic lipid flippase Drs2p-Cdc50p. *Nat Commun* **10**:4142. doi:10.1038/s41467-019-12191-9

Bai L, You Q, Jain BK, Duan HD, Kovach A, Graham TR, Li H. 2020. Transport mechanism of P4 ATPase phosphatidylcholine flippases. *eLife* **9**:e62163. doi:10.7554/eLife.62163

Balla T. 2013. Phosphoinositides: tiny lipids with giant impact on cell regulation. *Physiol Rev* **93**:1019–1137. doi:10.1152/physrev.00028.2012

Bohdanowicz M, Grinstein S. 2013. Role of phospholipids in endocytosis, phagocytosis, and macropinocytosis. *Physiol Rev* **93**:69–106. doi:10.1152/physrev.00002.2012

Bretscher MS. 1972. Asymmetrical lipid bilayer structure for biological membranes. *Nature New Biol* **236**:11–12. doi:10.1038/newbio236011a0

Bryde S, Hennrich H, Verhulst PM, Devaux PF, Lenoir G, Holthuis JCM. 2010. CDC50 proteins are critical components of the human class-1 P4-ATPase transport machinery. *J Biol Chem* **285**:40562–40572. doi:10.1074/jbc.M110.139543

Bull LN, van Eijk MJ, Pawlikowska L, DeYoung JA, Juijn JA, Liao M, Klomp LW, Lomri N, Berger R, Scharschmidt BF, Knisely AS, Houwen RH, Freimer NB. 1998. A gene encoding a P-type ATPase mutated in two forms of hereditary cholestasis. *Nat Genet* **18**:219–224. doi:10.1038/ng0398-219

Chalat M, Moleschi K, Molday RS. 2017. C-terminus of the P4-ATPase ATP8A2 functions in protein folding and regulation of phospholipid flippase activity. *Mol Biol Cell* **28**:452–462.

773 doi:10.1091/mbc.E16-06-0453
774 Chen VB, Arendall WB, Headd JJ, Keedy DA, Immormino RM, Kapral GJ, Murray LW, Richardson
775 JS, Richardson DC. 2010. MolProbity: all-atom structure validation for macromolecular
776 crystallography. *Acta Crystallogr D Biol Crystallogr* **66**:12–21. doi:10.1107/S0907444909042073
777 Clark J, Anderson KE, Juvin V, Smith TS, Karpe F, Wakelam MJO, Stephens LR, Hawkins PT. 2011.
778 Quantification of PtdInsP3 molecular species in cells and tissues by mass spectrometry. *Nat*
779 *Methods* **8**:267–272. doi:10.1038/nmeth.1564
780 Coleman JA, Molday RS. 2011. Critical role of the beta-subunit CDC50A in the stable expression,
781 assembly, subcellular localization, and lipid transport activity of the P4-ATPase ATP8A2. *J Biol*
782 *Chem* **286**:17205–17216. doi:10.1074/jbc.M111.229419
783 Danko S, Daiho T, Yamasaki K, Liu X, Suzuki H. 2009. Formation of the stable structural analog of
784 ADP-sensitive phosphoenzyme of Ca2+-ATPase with occluded Ca2+ by beryllium fluoride: structural
785 changes during phosphorylation and isomerization. *J Biol Chem* **284**:22722–22735.
786 doi:10.1074/jbc.M109.029702
787 Deng B-C, Lv S, Cui W, Zhao R, Lu X, Wu J, Liu P. 2012. Novel ATP8B1 mutation in an adult male
788 with progressive familial intrahepatic cholestasis. *World J Gastroenterol* **18**:6504–6509.
789 doi:10.3748/wjg.v18.i44.6504
790 Dickson EJ, Hille B. 2019. Understanding phosphoinositides: rare, dynamic, and essential
791 membrane phospholipids. *Biochem J* **476**:1–23. doi:10.1042/BCJ20180022
792 Dixon PH, Sambrotta M, Chambers J, Taylor-Harris P, Syngelaki A, Nicolaides K, Knisely AS,
793 Thompson RJ, Williamson C. 2017. An expanded role for heterozygous mutations of ABCB4,
794 ABCB11, ATP8B1, ABCC2 and TJP2 in intrahepatic cholestasis of pregnancy. *Sci Rep* **7**:11823.
795 doi:10.1038/s41598-017-11626-x
796 Ekberg K, Palmgren MG, Veierskov B, Buch-Pedersen MJ. 2010. A novel mechanism of P-type
797 ATPase autoinhibition involving both termini of the protein. *J Biol Chem* **285**:7344–7350.
798 doi:10.1074/jbc.M109.096123
799 Emsley P, Lohkamp B, Scott WG, Cowtan K. 2010. Features and development of Coot. *Acta*
800 *Crystallogr D Biol Crystallogr* **66**:486–501. doi:10.1107/S0907444910007493
801 Gantzel RH, Mogensen LS, Mikkelsen SA, Vilsen B, Molday RS, Vestergaard AL, Andersen JP.
802 2017. Disease mutations reveal residues critical to the interaction of P4-ATPases with lipid
803 substrates. *Sci Rep* **7**:10418. doi:10.1038/s41598-017-10741-z
804 Gautherot J, Delautier D, Maubert M-A, Aït-Slimane T, Bolbach G, Delaunay J-L, Durand-Schneider
805 A-M, Firrincieli D, Barbu V, Chignard N, Housset C, Maurice M, Falguières T. 2014. Phosphorylation
806 of ABCB4 impacts its function: insights from disease-causing mutations. *Hepatol Baltim Md* **60**:610–
807 621. doi:10.1002/hep.27170

808 Gautherot J, Durand-Schneider A-M, Delautier D, Delaunay J-L, Rada A, Gabillet J, Housset C,
809 Maurice M, Aït-Slimane T. 2012. Effects of cellular, chemical, and pharmacological chaperones on
810 the rescue of a trafficking-defective mutant of the ATP-binding cassette transporter proteins
811 ABCB1/ABCB4. *J Biol Chem* **287**:5070–5078. doi:10.1074/jbc.M111.275438
812 Hancock JF, Paterson H, Marshall CJ. 1990. A polybasic domain or palmitoylation is required in
813 addition to the CAAX motif to localize p21ras to the plasma membrane. *Cell* **63**:133–139.
814 doi:10.1016/0092-8674(90)90294-o
815 Hanson PK, Malone L, Birchmore JL, Nichols JW. 2003. Lem3p is essential for the uptake and
816 potency of alkylphosphocholine drugs, edelfosine and miltefosine. *J Biol Chem* **278**:36041–36050.
817 doi:10.1074/jbc.M305263200
818 Hiraizumi M, Yamashita K, Nishizawa T, Nureki O. 2019. Cryo-EM structures capture the transport
819 cycle of the P4-ATPase flippase. *Science* **365**:1149–1155. doi:10.1126/science.aay3353
820 Holemans T, Sørensen DM, van Veen S, Martin S, Hermans D, Kemmer GC, Van den Haute C,
821 Baekelandt V, Günther Pomorski T, Agostinis P, Wuytack F, Palmgren M, Eggermont J, Vangheluwe
822 P. 2015. A lipid switch unlocks Parkinson's disease-associated ATP13A2. *Proc Natl Acad Sci U S A*
823 **112**:9040–9045. doi:10.1073/pnas.1508220112
824 Huttlin EL, Jedrychowski MP, Elias JE, Goswami T, Rad R, Beausoleil SA, Villén J, Haas W, Sowa
825 ME, Gygi SP. 2010. A tissue-specific atlas of mouse protein phosphorylation and expression. *Cell*
826 **143**:1174–1189. doi:10.1016/j.cell.2010.12.001
827 Jacquemin E. 2012. Progressive familial intrahepatic cholestasis. *Clin Res Hepatol Gastroenterol* **36**
828 **Suppl 1**:S26-35. doi:10.1016/S2210-7401(12)70018-9
829 Jacquot A, Montigny C, Hennrich H, Barry R, le Maire M, Jaxel C, Holthuis J, Champeil P, Lenoir G.
830 2012. Phosphatidylserine stimulation of Drs2p·Cdc50p lipid translocase dephosphorylation is
831 controlled by phosphatidylinositol-4-phosphate. *J Biol Chem* **287**:13249–13261.
832 doi:10.1074/jbc.M111.313916
833 Klodos I, Esmann M, Post RL. 2002. Large-scale preparation of sodium-potassium ATPase from
834 kidney outer medulla. *Kidney Int* **62**:2097–2100. doi:10.1046/j.1523-1755.2002.00654.x
835 Klomp LWJ, Vargas JC, van Mil SWC, Pawlikowska L, Strautnieks SS, van Eijk MJT, Juijn JA,
836 Pabón-Peña C, Smith LB, DeYoung JA, Byrne JA, Gombert J, van der Brugge G, Berger R,
837 Jankowska I, Pawlowska J, Villa E, Knisely AS, Thompson RJ, Freimer NB, Houwen RHJ, Bull LN.
838 2004. Characterization of mutations in ATP8B1 associated with hereditary cholestasis. *Hepatol*
839 *Baltim Md* **40**:27–38. doi:10.1002/hep.20285
840 Kobayashi T, Menon AK. 2018. Transbilayer lipid asymmetry. *Curr Biol CB* **28**:R386–R391.
841 doi:10.1016/j.cub.2018.01.007
842 Kubitz R, Sütfels G, Kühlkamp T, Kölling R, Häussinger D. 2004. Trafficking of the bile salt export

843 pump from the Golgi to the canalicular membrane is regulated by the p38 MAP kinase.
844 *Gastroenterology* **126**:541–553. doi:10.1053/j.gastro.2003.11.003
845 Lee S, Uchida Y, Wang J, Matsudaira T, Nakagawa T, Kishimoto T, Mukai K, Inaba T, Kobayashi T,
846 Molday RS, Taguchi T, Arai H. 2015. Transport through recycling endosomes requires EHD1
847 recruitment by a phosphatidylserine translocase. *EMBO J* **34**:669–688.
848 doi:10.15252/embj.201489703
849 Lemmon MA. 2008. Membrane recognition by phospholipid-binding domains. *Nat Rev Mol Cell Biol*
850 **9**:99–111. doi:10.1038/nrm2328
851 Lenoir G, Williamson P, Puts CF, Holthuis JCM. 2009. Cdc50p plays a vital role in the ATPase
852 reaction cycle of the putative aminophospholipid transporter Drs2p. *J Biol Chem* **284**:17956–17967.
853 doi:10.1074/jbc.M109.013722
854 Leventis PA, Grinstein S. 2010. The distribution and function of phosphatidylserine in cellular
855 membranes. *Annu Rev Biophys* **39**:407–427. doi:10.1146/annurev.biophys.093008.131234
856 Li P, Wang K, Salustros N, Grønberg C, Gourdon P. 2021. Structure and transport mechanism of
857 P5B-ATPases. *Nat Commun* **12**:3973. doi:10.1038/s41467-021-24148-y
858 López-Marqués RL, Poulsen LR, Bailly A, Geisler M, Pomorski TG, Palmgren MG. 2015. Structure
859 and mechanism of ATP-dependent phospholipid transporters. *Biochim Biophys Acta* **1850**:461–475.
860 doi:10.1016/j.bbagen.2014.04.008
861 Lyons JA, Timcenko M, Dieudonné T, Lenoir G, Nissen P. 2020. P4-ATPases: how an old dog learnt
862 new tricks - structure and mechanism of lipid flippases. *Curr Opin Struct Biol* **63**:65–73.
863 doi:10.1016/j.sbi.2020.04.001
864 Marat AL, Haucke V. 2016. Phosphatidylinositol 3-phosphates-at the interface between cell
865 signalling and membrane traffic. *EMBO J* **35**:561–579. doi:10.15252/embj.201593564
866 Montigny C, Lyons J, Champeil P, Nissen P, Lenoir G. 2016. On the molecular mechanism of
867 flippase- and scramblase-mediated phospholipid transport. *Biochim Biophys Acta* **1861**:767–783.
868 doi:10.1016/j.bbalip.2015.12.020
869 Muñoz-Martínez F, Torres C, Castanys S, Gamarro F. 2010. CDC50A plays a key role in the uptake
870 of the anticancer drug perifosine in human carcinoma cells. *Biochem Pharmacol* **80**:793–800.
871 doi:10.1016/j.bcp.2010.05.017
872 Murate M, Abe M, Kasahara K, Iwabuchi K, Umeda M, Kobayashi T. 2015. Transbilayer distribution
873 of lipids at nano scale. *J Cell Sci* **128**:1627–1638. doi:10.1242/jcs.163105
874 Nakanishi H, Nishizawa T, Segawa K, Nureki O, Fujiyoshi Y, Nagata S, Abe K. 2020. Transport
875 Cycle of Plasma Membrane Flippase ATP11C by Cryo-EM. *Cell Rep* **32**:108208.
876 doi:10.1016/j.celrep.2020.108208
877 Natarajan P, Liu K, Patil DV, Sciorra VA, Jackson CL, Graham TR. 2009. Regulation of a Golgi

878 flippase by phosphoinositides and an ArfGEF. *Nat Cell Biol* **11**:1421–1426. doi:10.1038/ncb1989
879 Noe J, Hagenbuch B, Meier PJ, St-Pierre MV. 2001. Characterization of the mouse bile salt export
880 pump overexpressed in the baculovirus system. *Hepatology* **33**:1223–1231.
881 doi:10.1053/jhep.2001.24171
882 Onat OE, Gulsuner S, Bilguvar K, Nazli Basak A, Topaloglu H, Tan M, Tan U, Gunel M, Ozcelik T.
883 2013. Missense mutation in the ATPase, aminophospholipid transporter protein ATP8A2 is
884 associated with cerebellar atrophy and quadrupedal locomotion. *Eur J Hum Genet EJHG* **21**:281–
885 285. doi:10.1038/ejhg.2012.170
886 Painter JN, Savander M, Ropponen A, Nupponen N, Riikonen S, Ylikorkala O, Lehesjoki A-E,
887 Aittomäki K. 2005. Sequence variation in the ATP8B1 gene and intrahepatic cholestasis of
888 pregnancy. *Eur J Hum Genet EJHG* **13**:435–439. doi:10.1038/sj.ejhg.5201355
889 Pd A, Pv A, G B, Vb C, Iw D, N E, Jj H, Lw H, Gj K, Rw G-K, Aj M, Nw M, R O, Rj R, Dc R, Js R, Tc
890 T, Ph Z. 2010. PHENIX: a comprehensive Python-based system for macromolecular structure
891 solution. *Acta Crystallogr D Biol Crystallogr* **66**. doi:10.1107/S0907444909052925
892 Pettersen EF, Goddard TD, Huang CC, Meng EC, Couch GS, Croll TI, Morris JH, Ferrin TE. 2021.
893 UCSF ChimeraX: Structure visualization for researchers, educators, and developers. *Protein Sci*
894 *Publ Protein Soc* **30**:70–82. doi:10.1002/pro.3943
895 Platre MP, Bayle V, Armengot L, Bareille J, Marquès-Bueno MDM, Creff A, Maneta-Peyret L, Fiche
896 J-B, Nollmann M, Miège C, Moreau P, Martinière A, Jaillais Y. 2019. Developmental control of plant
897 Rho GTPase nano-organization by the lipid phosphatidylserine. *Science* **364**:57–62.
898 doi:10.1126/science.aav9959
899 Pomorski T, Lombardi R, Riezman H, Devaux PF, van Meer G, Holthuis JCM. 2003. Drs2p-related
900 P-type ATPases Dnf1p and Dnf2p are required for phospholipid translocation across the yeast
901 plasma membrane and serve a role in endocytosis. *Mol Biol Cell* **14**:1240–1254.
902 doi:10.1091/mbc.e02-08-0501
903 Pomorski TG, Menon AK. 2016. Lipid somersaults: Uncovering the mechanisms of protein-mediated
904 lipid flipping. *Prog Lipid Res* **64**:69–84. doi:10.1016/j.plipres.2016.08.003
905 Post RL, Hegyvary C, Kume S. 1972. Activation by adenosine triphosphate in the phosphorylation
906 kinetics of sodium and potassium ion transport adenosine triphosphatase. *J Biol Chem* **247**:6530–
907 6540.
908 Poulsen LR, López-Marqués RL, McDowell SC, Okkeri J, Licht D, Schulz A, Pomorski T, Harper JF,
909 Palmgren MG. 2008. The Arabidopsis P4-ATPase ALA3 localizes to the golgi and requires a beta-
910 subunit to function in lipid translocation and secretory vesicle formation. *Plant Cell* **20**:658–676.
911 doi:10.1105/tpc.107.054767
912 Punjani A, Rubinstein JL, Fleet DJ, Brubaker MA. 2017. cryoSPARC: algorithms for rapid

913 unsupervised cryo-EM structure determination. *Nat Methods* **14**:290–296. doi:10.1038/nmeth.4169
914 Punjani A, Zhang H, Fleet DJ. 2020. Non-uniform refinement: adaptive regularization improves
915 single-particle cryo-EM reconstruction. *Nat Methods* **17**:1214–1221. doi:10.1038/s41592-020-
916 00990-8
917 Riekhof WR, Wu J, Gijón MA, Zarini S, Murphy RC, Voelker DR. 2007. Lysophosphatidylcholine
918 metabolism in Saccharomyces cerevisiae: the role of P-type ATPases in transport and a broad
919 specificity acyltransferase in acylation. *J Biol Chem* **282**:36853–36861.
920 doi:10.1074/jbc.M706718200
921 Saffioti NA, de Sautu M, Riesco AS, Ferreira-Gomes MS, Rossi JPFC, Mangialavori IC. 2021.
922 Conformational changes during the reaction cycle of plasma membrane Ca2+-ATPase in the
923 autoinhibited and activated states. *Biochem J* **478**:2019–2034. doi:10.1042/BCJ20210036
924 Saito K, Fujimura-Kamada K, Furuta N, Kato U, Umeda M, Tanaka K. 2004. Cdc50p, a protein
925 required for polarized growth, associates with the Drs2p P-type ATPase implicated in phospholipid
926 translocation in Saccharomyces cerevisiae. *Mol Biol Cell* **15**:3418–3432. doi:10.1091/mbc.e03-11-
927 0829
928 Segawa K, Kikuchi A, Noji T, Sugiura Y, Hiraga K, Suzuki C, Haginoya K, Kobayashi Y, Matsunaga
929 M, Ochiai Y, Yamada K, Nishimura T, Iwasawa S, Shoji W, Sugihara F, Nishino K, Kosako H, Ikawa
930 M, Uchiyama Y, Suematsu M, Ishikita H, Kure S, Nagata S. 2021. A sublethal ATP11A mutation
931 associated with neurological deterioration causes aberrant phosphatidylcholine flipping in plasma
932 membranes. *J Clin Invest* **131**:148005. doi:10.1172/JCI148005
933 Segawa K, Kurata S, Nagata S. 2018. The CDC50A extracellular domain is required for forming a
934 functional complex with and chaperoning phospholipid flippases to the plasma membrane. *J Biol*
935 *Chem* **293**:2172–2182. doi:10.1074/jbc.RA117.000289
936 Takatsu H, Tanaka G, Segawa K, Suzuki J, Nagata S, Nakayama K, Shin H-W. 2014. Phospholipid
937 flippase activities and substrate specificities of human type IV P-type ATPases localized to the
938 plasma membrane. *J Biol Chem* **289**:33543–33556. doi:10.1074/jbc.M114.593012
939 Terwilliger TC, Sobolev OV, Afonine PV, Adams PD. 2018. Automated map sharpening by
940 maximization of detail and connectivity. *Acta Crystallogr Sect Struct Biol* **74**:545–559.
941 doi:10.1107/S2059798318004655
942 Timcenko M, Dieudonné T, Montigny C, Boesen T, Lyons JA, Lenoir G, Nissen P. 2021. Structural
943 Basis of Substrate-Independent Phosphorylation in a P4-ATPase Lipid Flippase. *J Mol Biol* 167062.
944 doi:10.1016/j.jmb.2021.167062
945 Timcenko M, Lyons JA, Januliene D, Ulstrup JJ, Dieudonné T, Montigny C, Ash M-R, Karlsen JL,
946 Boesen T, Kühlbrandt W, Lenoir G, Moeller A, Nissen P. 2019. Structure and autoregulation of a P4-
947 ATPase lipid flippase. *Nature* **571**:366–370. doi:10.1038/s41586-019-1344-7

948 Tsai P-C, Hsu J-W, Liu Y-W, Chen K-Y, Lee F-JS. 2013. Arl1p regulates spatial membrane
949 organization at the trans-Golgi network through interaction with Arf-GEF Gea2p and flippase Drs2p.
950 *Proc Natl Acad Sci U S A* **110**:E668-677. doi:10.1073/pnas.1221484110
951 van der Mark VA, Elferink RPJO, Paulusma CC. 2013. P4 ATPases: flippases in health and disease.
952 *Int J Mol Sci* **14**:7897–7922. doi:10.3390/ijms14047897
953 van der Velden LM, Wichers CGK, van Breevoort AED, Coleman JA, Molday RS, Berger R, Klomp
954 LWJ, van de Graaf SFJ. 2010. Heteromeric interactions required for abundance and subcellular
955 localization of human CDC50 proteins and class 1 P4-ATPases. *J Biol Chem* **285**:40088–40096.
956 doi:10.1074/jbc.M110.139006
957 van Meer G. 2011. Dynamic transbilayer lipid asymmetry. *Cold Spring Harb Perspect Biol* **3**.
958 doi:10.1101/cshperspect.a004671
959 van Meer G, Voelker DR, Feigenson GW. 2008. Membrane lipids: where they are and how they
960 behave. *Nat Rev Mol Cell Biol* **9**:112–124. doi:10.1038/nrm2330
961 Verkleij AJ, Zwaal RF, Roelofsen B, Comfurius P, Kastelijn D, van Deenen LL. 1973. The asymmetric
962 distribution of phospholipids in the human red cell membrane. A combined study using
963 phospholipases and freeze-etch electron microscopy. *Biochim Biophys Acta* **323**:178–193.
964 doi:10.1016/0005-2736(73)90143-0
965 Vestergaard AL, Coleman JA, Lemmin T, Mikkelsen SA, Molday LL, Vilsen B, Molday RS, Dal Peraro
966 M, Andersen JP. 2014. Critical roles of isoleucine-364 and adjacent residues in a hydrophobic gate
967 control of phospholipid transport by the mammalian P4-ATPase ATP8A2. *Proc Natl Acad Sci U S A*
968 **111**:E1334-1343. doi:10.1073/pnas.1321165111
969 Villén J, Beausoleil SA, Gerber SA, Gygi SP. 2007. Large-scale phosphorylation analysis of mouse
970 liver. *Proc Natl Acad Sci U S A* **104**:1488–1493. doi:10.1073/pnas.0609836104
971 Yang J, Yan R, Roy A, Xu D, Poisson J, Zhang Y. 2015. The I-TASSER Suite: protein structure and
972 function prediction. *Nat Methods* **12**:7–8. doi:10.1038/nmeth.3213
973 Yeung T, Heit B, Dubuisson J-F, Fairn GD, Chiu B, Inman R, Kapus A, Swanson M, Grinstein S.
974 2009. Contribution of phosphatidylserine to membrane surface charge and protein targeting during
975 phagosome maturation. *J Cell Biol* **185**:917–928. doi:10.1083/jcb.200903020
976 Zhou X, Sebastian TT, Graham TR. 2013. Auto-inhibition of Drs2p, a yeast phospholipid flippase, by
977 its carboxyl-terminal tail. *J Biol Chem* **288**:31807–31815. doi:10.1074/jbc.M113.481986
978
979